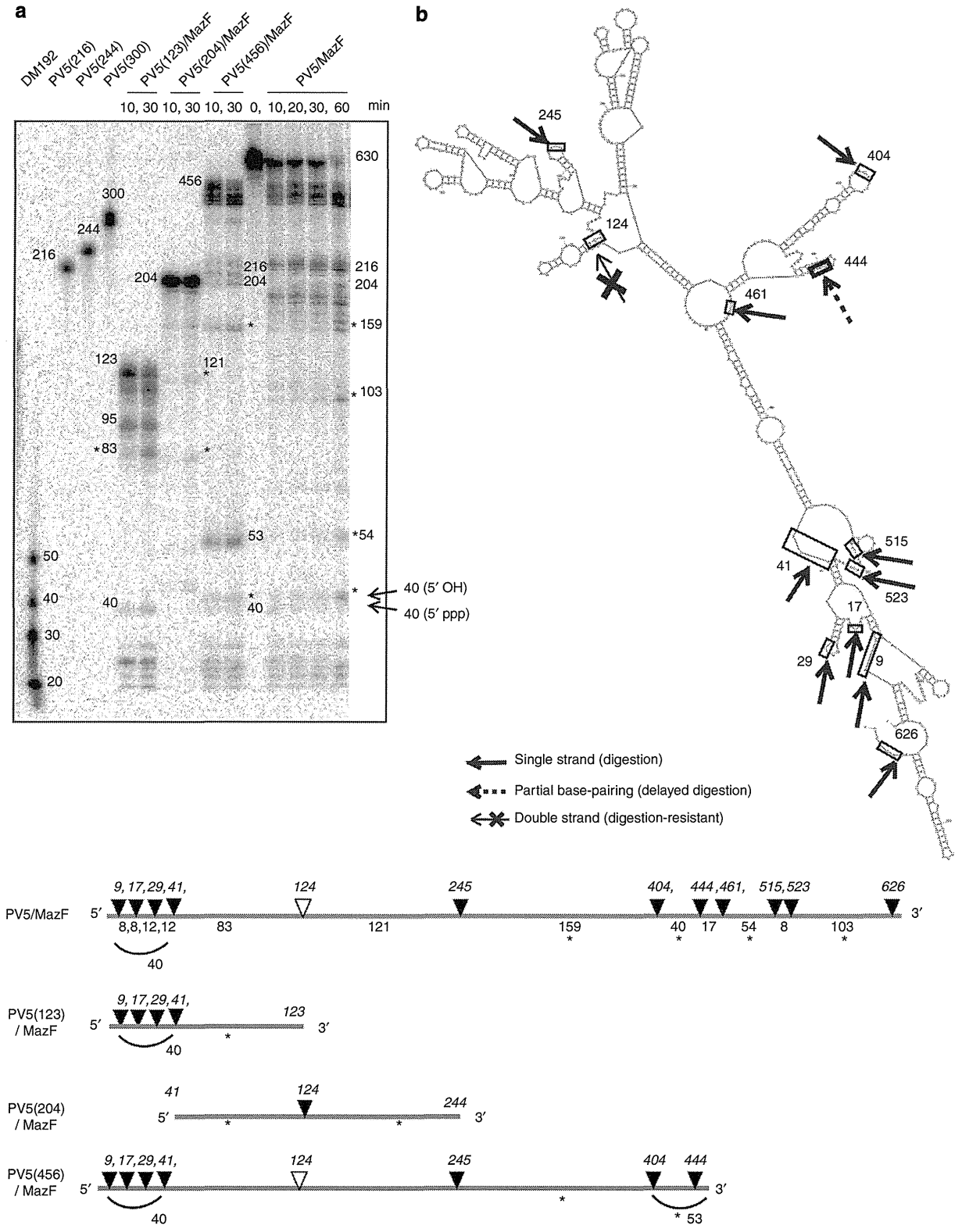

Figure 6 | Partial digestion of PV5 with MazF. (**a**) MazF-induced cleavage pattern of PV5 and the deletion mutants visualized on a denaturing 5% PAGE. PV5 was digested with MazF at room temperature, and other RNAs were digested at 37 °C. The cleavage pattern is schematically drawn at the bottom of the figure. MazF recognized ACA-cleavage sites are indicated by triangles. Black triangles indicate the observed cleavage sites and white triangles indicate sites not detected on the gel. Asterisks indicate the fragments produced by MazF-mediated ACA-specific digestion. Italic letters show the position numbers of the first A residues in ACA sequences of PV5. RNA size markers: DM192 (20-, 30-, 40- or 50-mer, Bio Dynamics Laboratory Inc.), PV5(216)(216-mer), PV5(244)(244-mer) and PV5(300)(300-mer). (**b**) Secondary structure of PV5 predicted by the mfold software. Rectangles show the ACA sites of PV5. The position numbers of the first A residues in ACA sequences of PV5 are shown. Solid arrows indicate the MazF-digestion sites. Broken arrow indicates the delayed digestion site.

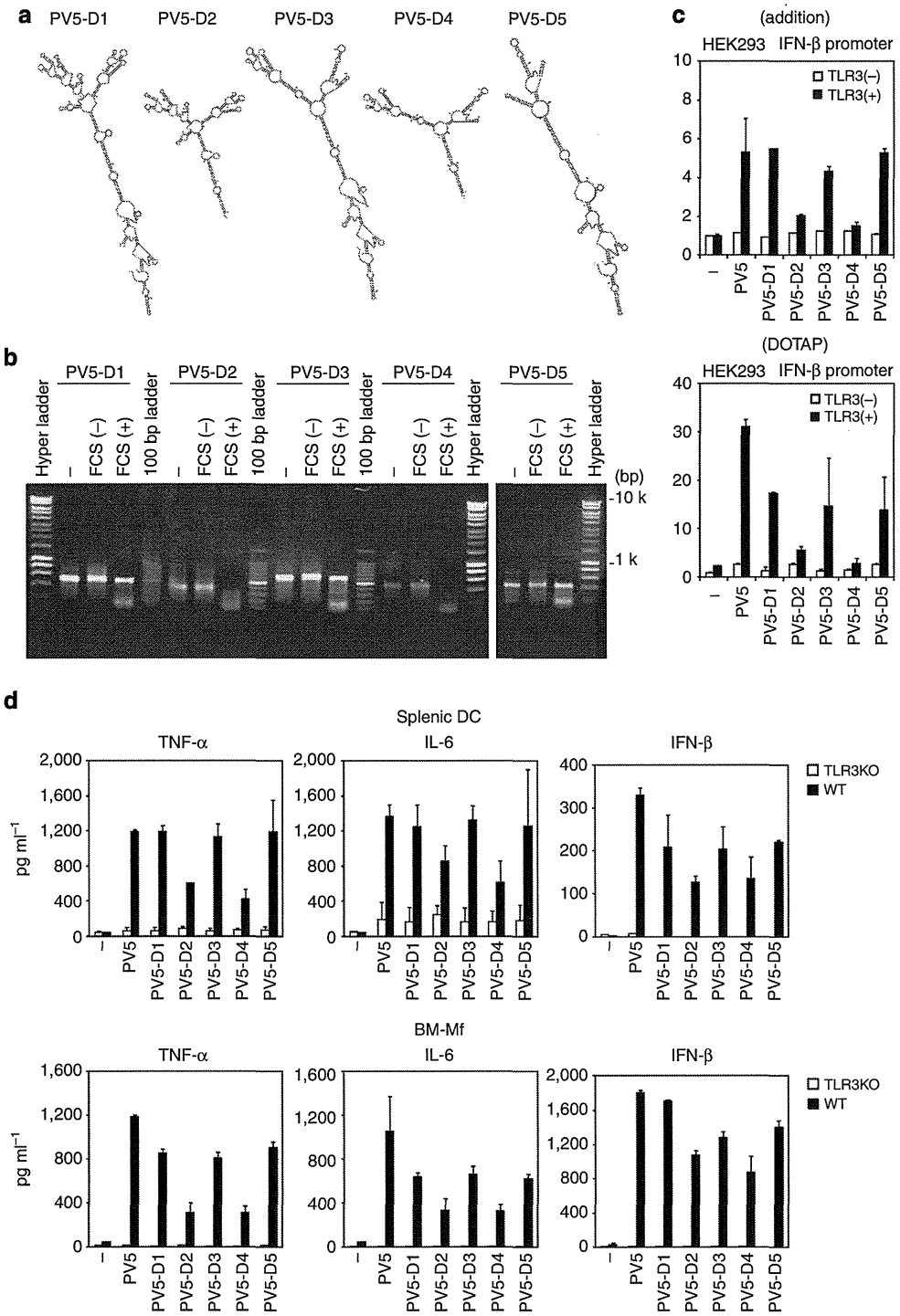

Figure 7 | Mapping of TLR3-activating RNA structure in PV5. (**a**) Secondary structure of PV5-derived RNAs (PV5-D1–PV5-D5) predicted by the mfold software. (**b**) RNAs were incubated in FCS-free or -containing medium at 37 °C. Non-treated RNA or RNA incubated for 30 min were loaded onto a 1% agarose gel. (**c**) TLR3-mediated IFN-β promoter activation induced by PV5 or PV5-derived RNAs in HEK293 cells transiently expressing TLR3. Cells were stimulated with indicated RNAs (10 μg ml^{-1}) (upper panel) or RNAs complexed with DOTAP (1 μg ml^{-1}) (lower panel). After 6 h, luciferase reporter activity was measured and expressed as the fold induction relative to the activity of unstimulated cells. Data are shown as the mean ± s.d. Representative data from three independent experiments are shown. (**d**) Splenic CD11c^{+} DCs (upper panels) or bone marrow-derived macrophages (lower panels) (2×10^6 per ml) isolated from TLR3$^{-/-}$ or WT mice were stimulated with 100 pmol ml^{-1} PV5 or PV5-derived RNAs in FCS-free AIM medium. Twenty-four hours after stimulation, culture supernatants were collected, and IFN-β in the supernatants was quantified using ELISA. TNF-α and IL-6 levels were measured using CBA. Representative data from three independent experiments are shown (mean ± s.d.).

to activate TLR3 was dependent on the dsRNA region within the RNA molecule, which is required for interaction with the N- and C-terminal dsRNA-binding sites of the TLR3 ECD. Based on the structural analysis of the TLR3–dsRNA complex, it has been proposed that 40–50 bp dsRNA was the minimum signalling unit with two TLR3 molecules[31]. Jelinek *et al.*[11] reported that dsRNAs,

>90 bp in length, triggered TLR3 oligomerization and efficiently induced IFN-β and TNF-α production in conventional murine DCs. Functional PV-RNAs, such as PV5 and PV6, induced TLR3-dependent IFN-α/β and proinflammatory cytokines from mouse CD11c$^+$ DCs (Fig. 5); these RNAs appeared to oligomerize TLR3 molecules even though they harbour bulges and internal loops in their duplex structures. If this is the case, TLR3 recognizes not only perfect duplex of ~90 bp dsRNA but also the mismatched RNA duplex whithin ~600-nt PV-RNA. We identified the core RNA structure required for TLR3 activation in PV5, which is relatively long stem structure with bulge and internal loops typically shown in PV5-D5 mfold secondary structure. The fascinated model for TLR3 dimer formation has been proposed, in which shorter RNA duplexes of between 21 and 30 bp can form less stable complexes with two TLR3 molecules[32]. Thus, TLR3 appears to have flexibility to recognize RNA molecules.

Interestingly, PV5 segments (approximately 200 nts in length; PV5 a, b and c) lost the ability to activate TLR3 in HEK293 cells despite their degradation-resistant structure (Supplementary Fig. S3c), suggesting that an appropriate topology of multiple RNA duplexes are required for TLR3 activation. In addition, PV5-D2 and -D4 failed to activate IFN-β promoter in HEK293 cells expressing TLR3, but efficiently induced type I IFN and proinflammatory cytokine production from mouse splenic DCs and bone marrow-derived macrophages in a TLR3-dependent manner (Fig. 7). Recently, it has been reported that TLR3 undergoes cathepsin-mediated proteolytic processing, and both full-length and C-terminal cleaved form of TLR3 molecules reside in human retinal epithelial cell line and monocyte-derived DCs[38]. It is interesting if shorter RNAs with mismatched duplex, such as PV5-D2 and -D4, are recognized by protease-processed TLR3 in mouse DCs or bone marrow-derived macrophages with different binding modes from intact TLR3[38]. Indeed, the cleaved form of TLR3 is predominant in mouse macrophages[39], but less present in HEK293 cells[40], which may explain the different TLR3 responses to these RNAs between mouse DCs/macrophages and human HEK293 cells (Fig. 7).

There have been many reports indicating that TLR3-dependent inflammatory cytokine and chemokine production affects virus-induced pathology and host survival in RNA virus infections such as respiratory syncytial virus, influenza A virus and phlebovirus, a negative-strand RNA virus that produces minimal dsRNA as an intermediate product[8]. Furthermore, TLR3 functions as an endogenous sensor of necrosis and is required for chemokine production by peritoneal macrophages after co-culture with necrotic neutrophils[24]. However, these biological studies have suffered from the lack of information about the actual molecules sensed by TLR3 in such infection/inflammatory states. More recently, Bernard *et al.*[41] demonstrated that UV-damaged self-noncoding RNA is detected by TLR3. We suppose that viral/host RNAs with stable stem structures derived from infection- or inflammation-damaged cells activate TLR3 to induce cytokine and chemokine production.

In the case of PV infection, TLR3-mediated type I IFN production is important for viral clearance *in vivo*[15,16]. *In vitro* PV infection of splenic DCs promotes type I IFN production in a TLR3-dependent manner. The positive-stranded ssRNAs and the replicative form are robustly present in PV-infected cells, which might be segmented into functional ssRNAs similar to PV5 and PV6 extracellularly due to necrosis. Hence, in the local environment, segmented virus-derived structured RNAs can function as a TLR3 ligand. The flexible RNA-recognition mode of TLR3 may have some advantage to protect host against wide spectrum of virus infection.

Notably, RNA uptake is required for TLR3 signalling. Functional PV-RNAs possess the essential structural elements required for both cellular uptake and TLR3 oligomerization. We found that raftlin, a cytoplasmic lipid raft protein, is a molecule that participates in uptake of PV-RNAs and delivery to TLR3-positive early endosomes (Fig. 4). The features of the TLR3-recognizing PV-RNAs are consistent with our previous results that raftlin mediates poly(I:C) cellular uptake through interaction with the clathrin–AP-2 complex in human myeloid DCs and epithelial cells[35]. In addition, uptake of B/C-type CpG ODNs that share their uptake receptor with poly(I:C) was also mediated by raftlin[33,35]. Given that PV5-induced TLR3 activation in HEK293 cells was inhibited by pre-treatment with the B-type CpG ODN (Supplementary Fig. S5), PV5 likely utilizes the poly(I:C)/ODN-uptake receptor for endocytosis. Although CD14 and the scavenger receptor class A were reported to act as a poly(I:C)-uptake receptor in mouse macrophages and human bronchial epithelial cells, respectively[42,43], they did not participate in poly(I:C)/ODN cellular uptake in human DCs because of their absence on the cell surface[12]. There must be an additional uptake receptor for poly(I:C)/ODN. Identification of the uptake receptor for virus RNAs is important for improving our understanding of the innate immune response to viral infection and sterile inflammation.

TLRs recognize pathogen- or damage-associated molecular patterns and promote the activation of the innate and adaptive immune responses through ligand-induced oligomerization[44,45]. Structural analyses of TLR3, TLR4, TLR5, TLR2/1 and TLR2/6 ECDs, and their complexes with typical ligands, demonstrated that each TLR possessed ligand-binding sites or pockets and a dimerizing interface, which allowed for ligand-induced receptor dimerization[46,47]. Although there are multiple ligands for each TLR, it remains unknown whether they share common structural features. The current study is the first to characterize the RNA structure capable of triggering TLR3 activation and demonstrate that viral RNAs with intermittent stem structure are recognized by an uptake receptor and by TLR3, inducing innate immune signalling. Precise analyses of the mechanisms underlying pattern recognition by TLRs using different ligands might be important for engineering synthetic TLR-activating ligands.

Methods

Cell culture and reagents. HEK293 and Vero cells were maintained in DMEM (Invitrogen) supplemented with 10% heat-inactivated FCS (Invitrogen) and antibiotics. HeLa cells were kindly provided by Dr T. Fujita (Kyoto University) and maintained in Eagle's minimal essential medium (Nissui, Tokyo, Japan) supplemented with 1% L-glutamine and 5% heat-inactivated FCS. Normal embryonic lung fibroblasts, MRC5 cells, were maintained in MEM-alpha (Invitrogen) supplemented with 10% heat-inactivated FCS and antibiotics. The anti-human TLR3 monoclonal antibody (mAb) (clone TLR3.7) was generated in our laboratory[5]. The anti-human raftlin polyclonal Ab (pAb) and anti-mouse TLR3 mAb were kindly provided by Dr K. Saeki (Kyushu University) and Dr D. M. Segal (National Institutes of Health, MD), respectively.[34,11] Anti-EEA1 pAb (PA1-063) was purchased from Affinity Bioreagents; anti-β-actin mAb (A2228) was purchased from Sigma; the anti-LAMP1 mAb (328601) was purchased from Biolegend; the anti-TICAM-1 pAb (4596) was purchased from Cell Signaling; and Alexa Fluor-488 and -633-conjugated secondary antibodies were purchased from Invitrogen. Poly(I:C) was purchased from Amersham Biosciences. RNase A and RNase III were purchased from Ambion.

Mice. Inbred C57BL/6 WT mice were purchased from CLEA Japan (Tokyo, Japan). TLR3$^{-/-}$ mice were provided by Dr S. Akira (Osaka University). Mice were maintained under specific pathogen-free conditions in the animal facility of the Hokkaido University Graduate School of Medicine. Female mice of 6–10 week of age were used in all experiments that were performed according to the guidelines established by the Hokkaido University Animal Care and Use Committee.

Plasmids. The cDNA fragments encoding the open-reading frame of human TLR3 was amplified using RT–PCR with total RNA prepared from monocyte-derived DCs and was ligated into the cloning site of the expression vector, pEF-BOS, which was a gift from Dr S. Nagata (Kyoto University)[48]. Mahoney PV complementary

DNA was provided by Dr S. Koike (Tokyo Metropolitan Institute of Medical Science, Tokyo). TLR3-mutant plasmids were gifts from Dr K. Fukuda (Yamagata University)[29].

RNA extraction from PV-infected cells. Vero cells were infected with PV or not infected. Forty-eight hours later, cells and culture supernatants were divided by centrifugation (2,000 r.p.m., 10 min). TRIzol reagent (Invivogen) was added to cell pellets for extraction of RNA. Obtained RNAs were purified by ethanol precipitation, and concentration was determined by measuring the absorbance at 260 nm in a spectrophotometer.

Preparation of RNA. DNA fragments containing the PV gene segment and the T7 promoter sequence were amplified using PCR with specific primers and the PV-cDNA as a template (Supplementary Table S2). The PV sense and antisense RNAs from the PCR products were transcribed *in vitro* using an AmpliScribe T7 transcription kit (Epicentre Technologies, Madison, WI, USA) according to the manufacturer's protocol. The transcribed products were separated on a 1% agarose gel, and the band corresponding to PV RNA was excised using RECOCHIP (Takara). Then, eluted RNAs were ethanol precipitated and resuspended in RNase-free water. To generate dsRNA, sense and antisense RNAs were annealed. PV-ss/dsRNAs were pre-treated with polymyxin B (5 $\mu g\,ml^{-1}$) for 1 h before being added to mouse macrophages and DCs. RNA was labelled with Cy3 maleimide monoreactive dye (GE Healthcare) using the 5′ EndTag Nucleic Acid Labeling System (Vector Laboratories, Inc.). Cy3-PV5 showed a full activity.

Reporter gene assay. HEK293 cells (8×10^5 cells per well) were cultured in six-well plates and transfected with the TLR3-expression vector or an empty vector (400 ng per well), together with the reporter plasmid (400 ng per well) and an internal control vector phRL-TK (Promega, Madison, WI, USA) (20 ng per well) using FuGENE HD (Roche). The p-125 luc reporter containing the human IFN-β promoter region (-125 to $+19$) was provided by Dr T. Taniguchi (University of Tokyo). After 24 h, cells were collected and resusupended with FCS-free or -containing medium. Then, cells were seeded on 96-well plates and stimulated with the indicated RNAs. Six hours later, cells were lysed using the passive lysis buffer (Promega), and Firefly and *Renilla* luciferase activities were determined using a dual-luciferase reporter assay kit (Promega). The Firefly luciferase activity was normalized by *Renilla* luciferase activity and was expressed as the fold stimulation relative to activity in non-stimulated cells.

Filter binding assay. Radioisotope labelling of PV-RNAs by *in vitro* transcription with [α-^{32}P-ATP] was carried out as previously decribed[49]. Labelled PV-RNAs (2 nM) were mixed with varying concentrations (none or 6.25, 12.5 25, 50, 100 or 200 nM) of human TLR3 (amino acid 27–711; R&D Systems) and adjusted to a total volume of 25 μl using binding buffer (pH 5.0–7.0) containing 100 mM NaCl (20 mM AcONa (pH 5.0–6.0) or 20 mM Tris–HCl (pH 6.5–7.0)). After 30 min incubation, the mixtures were passed through a nitrocellulose filter and washed twice with 500 μl reaction buffer. The amount of bound RNA was measured using BAS 2500 (Fujifilm), and binding activities were calculated as the percentage of input RNA.

Quantitative PCR. Total RNA was extracted using the RNeasy mini kit (Qiagen, Valencia, CA) and reverse transcribed using the High Capacity cDNA Reverse Transcripition kit (Applied Biosystems) and random primers according to the manufacturer's instructions. qPCR was performed using the indicated primers (Supplementary Table S3) and the Step One Real-time PCR system (Applied Biosystems).

RNA interference and immunoblotting. siRNA duplexes (Raftlin, catalogue number s23219; negative control, catalogue number AM4635) were purchased from Ambion-Applied Biosystems. siRNA for TICAM-1 was purchased from Xeragon Inc. (Birmingham, AL, USA). HEK293 cells were cultured in 24-well plates and transfected with 20 pmol each siRNA, together with the expression vector for human TLR3 (200 ng), IFN-β promoter plasmid (100 ng) and an internal control vector (1.5 ng) using Lipofectamine 2000. Forty-eight hours after transfection, cells were stimulated with 10 $\mu g\,ml^{-1}$ ligands for 6 h. Cells were lysed and dual-luciferase activities were measured according to the manufacturer's instructions (Promega). Cell lysates were clarified by centrifugation and mixed with denaturing buffer. Samples were analysed using 10% SDS–PAGE followed by immunoblotting with anti-raftlin pAb (1/1,000), anti-β-actin mAb (1/1,000) or anti-TICAM-1 pAb (1/500). In the case of HeLa cells, cells cultured in 12-well plates were transfected with 40 pmol each siRNA using Lipofectamine 2000.

Confocal microscopy. HeLa cells (1.0×10^5 cells per well) were plated onto microcover glasses (Matsunami, Tokyo, Japan) in a 12-well plate. The following day, cells were incubated with 15 $\mu g\,ml^{-1}$ Cy3-labelled PV5 for 30 min at 4 °C. Cells were washed twice and further incubated for 5–60 min at 37 °C. At timed intervals, cells were fixed with 4% paraformaldehyde for 15 min and permeabilized using PBS containing 0.2% Triton and 1% BSA for 15 min. Fixed cells were labelled with anti-EEA1 pAb (1/200), anti-LAMP1 mAb (1/300) or anti-human TLR3 mAb (1/50) overnight at 4 °C. Then, Alexa Fluor-488- or -633-conjugated secondary Abs (1/400) were used to visualize the primary Abs. Prolong Gold was used for staining the nuclei. Cells were visualized at a $\times 63$ magnification using an LSM510 META microscope (Zeiss, Jena, Germany).

Purification of mouse DCs from spleen. Splenocytes from WT or TLR3$^{-/-}$ mice were treated with 400 IU MandleU per ml collagenase D (Roche) at 37 °C for 25 min in HBSS (Sigma-Aldrich). EDTA was added to the cell suspensions and incubated for an additional 5 min at 37 °C. After lysis of red blood cells using the ACK lysis buffer, splenocytes were incubated with magnetic-activated cell sorting anti-CD11c-conjugated microbeads, and DCs were purified using magnetic separation columns as indicated by the manufacturer (Miltenyi Biotec, Auburn, CA, USA). Positively selected cells were isolated and suspended in RPMI 1640 (Invitrogen) supplemented with 10% heat-inactivated FCS and antibiotics. For isolation of CD8α$^+$ DCs, the magnetic-activated cell sorting CD8α$^+$ DC-positive selection kit was used according to the manufacturer's instructions. Purity was checked routinely by FACS and was found to be $>80\%$ (CD11c$^+$) or $>90\%$ (CD8α$^+$), respectively.

Enzyme-linked immunosorbent assay and cytometric bead array. Cells were stimulated with the indicated RNAs in FCS-containing medium or FCS-free AIM-V medium (Invitrogen). Twenty-four hours after stimulation, culture supernatants were collected and analysed for cytokine levels with enzyme-linked immunosorbent assay (ELISA) or cytometric bead array (CBA). ELISA kits for IFN-α and IFN-β were purchased from PBL Biomedical Laboratories and were performed according to the manufacturer's instructions. CBA flex sets for mouse IL-6 and TNF-α were purchased from BD Bioscience. Experiments were performed according to the manufacturer's instructions, and samples were analysed using the FacsAria (BD Bioscience).

Statistical analysis. Statistical significance of differences between groups was determined by the Student's *t*-test.

Prediction of RNA secondary structure. The secondary structure of RNAs was modelled using mfold (http://mfold.rna.albany.edu/?q.mfold), RNAfold (http://rna.tbi.univie.ac.at/cgi-bin/RNAfold.cgi) and centroidfold program (http://www.ncrna.org/software/centroidfold/).

References

1. Stetson, D. B. & Medzhitov, R. Type I interferons in host defense. *Immunity* **25,** 373–381 (2006).
2. Vilcek, J. Fifty years of interferon research: aiming at a moving target. *Immunity* **25,** 343–348 (2006).
3. Akira, S., Uematsu, S. & Takeuchi, O. Pathogen recognition and innate immunity. *Cell* **124,** 783–801 (2006).
4. Alexopoulou, L., Holt, A. C., Medzhitov, R. & Flavell, R. A. Recognition of double stranded RNA and activation of NF-kappaB by Toll-like receptor 3. *Nature* **413,** 732–738 (2001).
5. Matsumoto, M., Kikkawa, S., Kohase, M., Miyake, K. & Seya, T. Establishment of monoclonal antibody against human Toll-like receptor 3 that blocks double-stranded RNA-mediated signaling. *Biochem. Biophys. Res. Commun.* **293,** 1364–1369 (2002).
6. Oshiumi, H., Matsumoto, M., Funami, K., Akazawa, T. & Seya, T. TICAM-1, an adaptor molecule that participates in Toll-like receptor 3-mediated interferon-β induction. *Nat. Immunol.* **4,** 161–167 (2003).
7. Yamamoto, M. *et al.* Role of adaptor TRIF in the MyD88-independent Toll-like receptor signaling pathway. *Science* **301,** 640–643 (2003).
8. Weber, F., Wagner, V., Rasmussen, S. B., Hartmann, R. & Paludan, S. R. Double-stranded RNA is produced by positive-stranded RNA viruses and DNA viruses but not in detectable amounts by negative-stranded RNA viruses. *J. Virol.* **80,** 5059–5064 (2006).
9. Matsumoto, M. *et al.* Subcellular localization of Toll-like receptor 3 in human dendritic cells. *J. Immunol.* **171,** 3154–3162 (2003).
10. Jongbloed, S. L. *et al.* Human CD141+ (BDCA-3)+ dendritic cells (DCs) represent a unique myeloid DC subset that cross-presents necrotic cell antigens. *J. Exp. Med.* **207,** 1247–1260 (2010).
11. Jelinek, I. *et al.* TLR3-specific double-stranded RNA oligonucleotide adjuvants induce dendritic cell cross-presentation, CTL responses, and antiviral protection. *J. Immunol.* **186,** 2422–2429 (2011).
12. Matsumoto, M. & Seya, T. TLR3: Interferon induction by double-stranded RNA including poly(I:C). *Adv. Drug. Deliv. Rev.* **60,** 805–812 (2008).
13. Hardarson, H. S. *et al.* Toll-like receptor 3 is an essential component of the innate stress response in virus-induced cardiac injury. *Am. J. Physio. Heart Circ. Physiol.* **292,** 251–258 (2007).

14. Negishi, H. *et al.* A critical link between Toll-like receptor 3 and type II interferon signaling pathways in antiviral innate immunity. *Proc. Natl Acad. Sci. USA* **105,** 20446–20451 (2008).
15. Oshiumi, H. *et al.* The TLR3-TICAM-1 pathway is mandatory for innate immune responses to poliovirus infection. *J. Immunol.* **187,** 5320–5327 (2011).
16. Abe, Y. *et al.* The Toll-like receptor 3-mediayed antiviral response is important for protection against poliovirus infection in poliovirus receptor transgenic mice. *J. Virol.* **86,** 185–194 (2012).
17. Zhang, S.-Y. *et al.* TLR3 deficiency in patients with herpes simplex encephalitis. *Science* **317,** 1522–1527 (2007).
18. Guo, Y. *et al.* Herpes simplex virus encephalitis in a patient with completeTLR3 deficiency: TLR3 is otherwise redundant in protective immunity. *J. Exp. Med.* **208,** 2083–2098 (2011).
19. Sancho-Shimizu, V. *et al.* Herpes simplex encephalitis in children with autosomal recessive and dominant TRIF deficiency. *J. Clin. Invest.* **121,** 4889–4902 (2011).
20. Wang, T. *et al.* Toll-like receptor 3 mediates West Nile virus entry into the brain causing lethal encephalitis. *Nat. Med.* **10,** 1366–1373 (2004).
21. Goffic, R. L. *et al.* Detrimental contribution of the Toll-like receptor (TLR) 3 to influenza A virus-induced acute pneumonia. *PLoS Pathog.* **2,** 526–535 (2006).
22. Gowen, B. B. *et al.* TLR3 deletion limits mortality and disease severity due to phlebovirus infection. *J. Immunol.* **177,** 6301–6307 (2006).
23. Karikó, K., Ni, H., Capodici, J., Lamphier, M. & Weissman, D. mRNA is an endogenous ligand for Toll-like receptor 3. *J. Biol. Chem.* **279,** 12542–12550 (2004).
24. Cavassani, K. A. *et al.* TLR3 is an endogenous sensor of tissue necrosis during acute inflammatory events. *J. Exp. Med.* **205,** 2609–2621 (2008).
25. Kato, H. *et al.* Differential roles of MDA5 and RIG-I helicases in the recognition of RNA viruses. *Nature* **441,** 101–105 (2006).
26. Racaniello, V. R. Picornaviridae: the viruses and their replication. In *Section II: Specific Virus Families: Fields Virology* 5th edn (eds Knipe, D. M. & Howley, P. M.) 795–838 (Lippincott Wiliams & Wilkins, 2007).
27. Leonard, J. N. *et al.* The TLR3 signaling complex forms by cooperative receptor dimerization. *Proc. Natl Acad. Sci. USA* **105,** 258–263 (2008).
28. Hofacker, I. *et al.* Fast folding and comparison of RNA secondary structures. *Monatsh. Chem.* **125,** 167–188 (1994).
29. Fukuda, K. *et al.* Modulation of double-stranded RNA recognition by the N-terminal histidine-rich region of the human Toll-like receptor 3. *J. Biol. Chem.* **283,** 22787–22794 (2008).
30. Bell, J. K. *et al.* Leucine-rich repeats and pathogen recognition in Toll-like receptors. *Trends Immunol.* **24,** 528–533 (2003).
31. Liu, L. *et al.* Structural basis of Toll-like receptor 3 signaling with double-stranded RNA. *Science* **320,** 379–381 (2008).
32. Pirher, N., Ivicak, K., Pohar, J., Bencina, M. & Jerala, R. A second binding site for double-stranded RNA in TLR3 and consequences for interferon activation. *Nat. Struct. Mol. Biol.* **15,** 761–763 (2008).
33. Itoh, K., Watanabe, A., Funami, K., Seya, T. & Matsumoto, M. The clathrin-mediated endocytic pathway participates in dsRNA-induced IFN-β production. *J. Immunol.* **181,** 5522–5529 (2008).
34. Saeki, K., Miura, Y., Aki, D., Kurosaki, T. & Yoshimura, A. The B cell-specific major raft protein, Raftlin, is necessary for the integrity of lipid raft and BCR signal transduction. *EMBO J.* **22,** 3015–3026 (2003).
35. Watanabe, A. *et al.* Raftlin is involved in the nucleocapture complex to induce poly(I:C)-mediated TLR3 activation. *J. Biol. Chem.* **286,** 10702–10711 (2011).
36. Zhang, Y. *et al.* MazF cleaves cellular mRNAs specifically at ACA to block protein synthesis in *Escherichia coli*. *Mo. Cell* **12,** 913–923 (2003).
37. Yamaguchi, Y. & Inouye, M. mRNA interferanses, sequence-specific endoribonucleases from the toxin-antitoxin systems. *Prog. Mol. Biol. Transl. Sci.* **85,** 467–500 (2009).
38. Garcia-Cattaneo, A. *et al.* Cleavage of Toll-like receptor 3 by cathepsins B and H is essential for signaling. *Proc. Natl Acad. Sci. USA* **109,** 9053–9058 (2012).
39. Ewald, S. E. *et al.* Nucleic acid recognition by Toll-like receptors is coupled to stepwise processing by cathepsins and asparagine endopeptidase. *J. Exp. Med.* **208,** 643–651 (2011).
40. Toscano, F. *et al.* Cleaved/associated TLR3 represents the primary form of the signaling receptor. *J. Immunol.* **190,** 764–773 (2013).
41. Bernard, J. J. *et al.* Ultraviolet radiation damages self noncoding RNA and is detected by TLR3. *Nat. Med.* **18,** 1286–1291 (2012).
42. Lee, H. K. S., Dunzendorfer, K., Soldau, K. & Tobias, P. S. Double-stranded RNA-mediated TLR3 activation is enhanced by CD14. *Immunity* **24,** 153–163 (2006).
43. Limmon, G. V. *et al.* Scavenger receptor class-A is a novel cell surface receptor for double-stranded RNA. *FASEB J.* **22,** 159–167 (2008).
44. Medzhitov, R. & Janeway, Jr C. A. Innate immunity: the virtues of a nonclonal system of recognition. *Cell* **91,** 295–298 (1997).
45. Kono, H. & Rock, K. L. How dying cells alert the immune system to danger. *Nat. Rev. Immunol.* **8,** 279–289 (2008).
46. Kang, J. Y. & Lee, J.-O. Structural biology of the Toll-like receptor family. *Annu. Rev. Biochem.* **80,** 917–941 (2011).
47. Yoon, S. I. *et al.* Structural basis of TLR5-flagellin recognition and signaling. *Science* **335,** 859–864 (2012).
48. Mizushima, S. & Nagata, S. pEF-BOS, a powerful mammalian expression vector. *Nucleic Acid Res.* **18,** 5322–5323 (1990).
49. Fukuda, K. *et al.* Isolation and characterization of RNA aptamers specific for the hepatitis C virus nonstructural protein 3 protease. *Eur. J. Biochem.* **267,** 3685–3694 (2000).

Acknowledgements

We are grateful to our laboratory members for their invaluable discussions. We also thank Dr S. Akira (Osaka University) for providing TLR3 $^{-/-}$ mice, Dr S. Koike (Tokyo Metropolitan Institute of Medical Science) for PV-cDNA, Dr D. M. Segal (National Institutes of Health) for anti-mouse TLR3 mAb, Dr K. Saeki (Kyushu University) for anti-raftlin antibody, Dr T. Taniguchi (University of Tokyo) for p-125 luc reporter plasmid, Dr S. Nagata (Kyoto University) for pEF-BOS expression vector and Dr K. Fukuda (Yamagata University) for TLR3-mutant plasmids. This work was supported in part by Grants-in-Aid from the Ministry of Education, Science, and Culture, the Ministry of Health, Labor, and Welfare of Japan, and by the Akiyama Life Science Foundation.

Author contributions

M.T. and M.M. conceived and designed the experiments. M.T. and F.N. performed the experiments. M.T., F.N., T.S. and M.M. analysed the data. M.T. and M.M. wrote the paper.

Additional information

Supplementary Information accompanies this paper at http://www.nature.com/naturecommunications

Competing financial interests: The authors declare no competing financial interests.

Reprints and permission information is available online at http://npg.nature.com/reprintsandpermissions/

How to cite this article: Tatematsu, M. *et al.* Toll-like receptor 3 recognizes incomplete stem structures in single-stranded viral RNA. *Nat. Commun.* 4:1833 doi: 10.1038/ncomms2857 (2013).

Immunology Letters 154 (2013) 12–17

Contents lists available at ScienceDirect

Immunology Letters

journal homepage: www.elsevier.com/locate/immlet

Efficient *in vivo* depletion of CD8$^+$ T lymphocytes in common marmosets by novel CD8 monoclonal antibody administration

Tomoyuki Yoshida[a,b,*,1], Saori Suzuki[b,1], Yuki Iwasaki[a], Akihisa Kaneko[b], Akatsuki Saito[b], Yuki Enomoto[b], Atsunori Higashino[b], Akino Watanabe[b], Juri Suzuki[b], Kenichi Inoue[b], Teiko Kuroda[b], Masahiko Takada[b], Ryoji Ito[c], Mamoru Ito[c], Hirofumi Akari[a,b,*]

[a] *Tsukuba Primate Research Center, National Institute of Biomedical Innovation, Hachimandai, Tsukuba, Ibaraki 305-0843, Japan*
[b] *Primate Research Institute, Kyoto University, Inuyama, Aichi 484-8506, Japan*
[c] *Central Institute for Experimental Animals, Tomomachi, Kawasaki 210-0821, Japan*

ARTICLE INFO

Article history:
Received 16 April 2013
Received in revised form 4 August 2013
Accepted 12 August 2013
Available online xxx

Keywords:
Monoclonal antibody
CD8 T lymphocyte
Common marmoset
In vivo depletion

ABSTRACT

In order to directly demonstrate the roles of CD8$^+$ T lymphocytes in non-human primates, *in vivo* depletion of the CD8$^+$ T cells by administration of a CD8-specific monoclonal antibody (mAb) is one of the crucial techniques. Recently, the common marmoset (*Callithrix jacchus*), which is classified as a New World monkey, has been shown useful as an experimental animal model for various human diseases such as multiple sclerosis, Parkinson's disease and a number of infectious diseases. Here we show that an anti-marmoset CD8 mAb 6F10, which we have recently established, efficiently depletes the marmoset CD8$^+$ T lymphocytes *in vivo*, *i.e.*, the administration of 6F10 induces drastic and specific reduction in the ratio of the CD8$^+$ T cell subset for at least three weeks or longer. Our finding will help understand the pivotal role of CD8$^+$ T cells *in vivo* in the control of human diseases.

1. Introduction

The use of non-human primates as experimental animal models is highly effective for research on human diseases. Non-human primates and humans share comparable immune systems as compared with mice and are suitable for the evaluation of innate and adaptive immune responses against several viruses [1,2]. On the other hand, there are also several issues with chimpanzees and macaques. The most prevalent being that the use of the chimpanzee is limited by ethical and financial restrictions [3–6].

A New World monkey, the common marmoset (*Callithrix jacchus*) has several advantages as an experimental animal model. The small size of the marmoset makes it easier to handle and reduces maintenance costs [7]. Recently, it has been reported that the marmoset model is a very useful tool in investigating multiple sclerosis (MS), rheumatoid arthritis (RA) and Parkinson's disease [8–10]. Moreover, the marmoset has an immune system similar to that of humans and is suitable for the evaluation of innate and adaptive immune responses against several viruses which efficiently replicate in the marmoset [11–14].

CD8$^+$ T lymphocytes are a vital component of the adaptive immune response and are crucial to the control and clearance of intracellular pathogens. These cells play critical roles in purging acute infections, limiting persistent infections, and conferring life-long protective immunity. In order to clarify the pivotal role of CD8$^+$ T cells in a variety of non-human primate models for human diseases, *in vivo* depletion of CD8$^+$ T cells by administration of a CD8-specific monoclonal antibody (mAb) is a straightforward technique, although it has been established in Old World monkeys but not in New World monkeys [15–21].

We recently established a novel mAb 6F10 specific for common marmoset CD8 [7]. In this study, we demonstrated for the first time in New World monkeys that the administration of the 6F10 mAb efficiently depleted CD8$^+$ T lymphocytes in marmosets.

2. Materials and methods

2.1. Animals

All animal studies were conducted in accordance with the protocols of experimental procedures that were approved by the Animal Welfare and Animal Care Committee of the Primate Research Institute of Kyoto University, Inuyama, Japan. A total of

* Corresponding authors at: Primate Research Institute, Kyoto University, Inuyama, Aichi 484-8506, Japan. Tel.: +81 568 63 0440; fax: +81 568 62 9559.
E-mail addresses: yoshida.tomoyuki.4w@kyoto-u.ac.jp (T. Yoshida), akari.hirofumi.5z@kyoto-u.ac.jp (H. Akari).
[1] These two authors contributed equally to this work.

0165-2478/$ – see front matter © 2013 Elsevier B.V. All rights reserved.
http://dx.doi.org/10.1016/j.imlet.2013.08.005

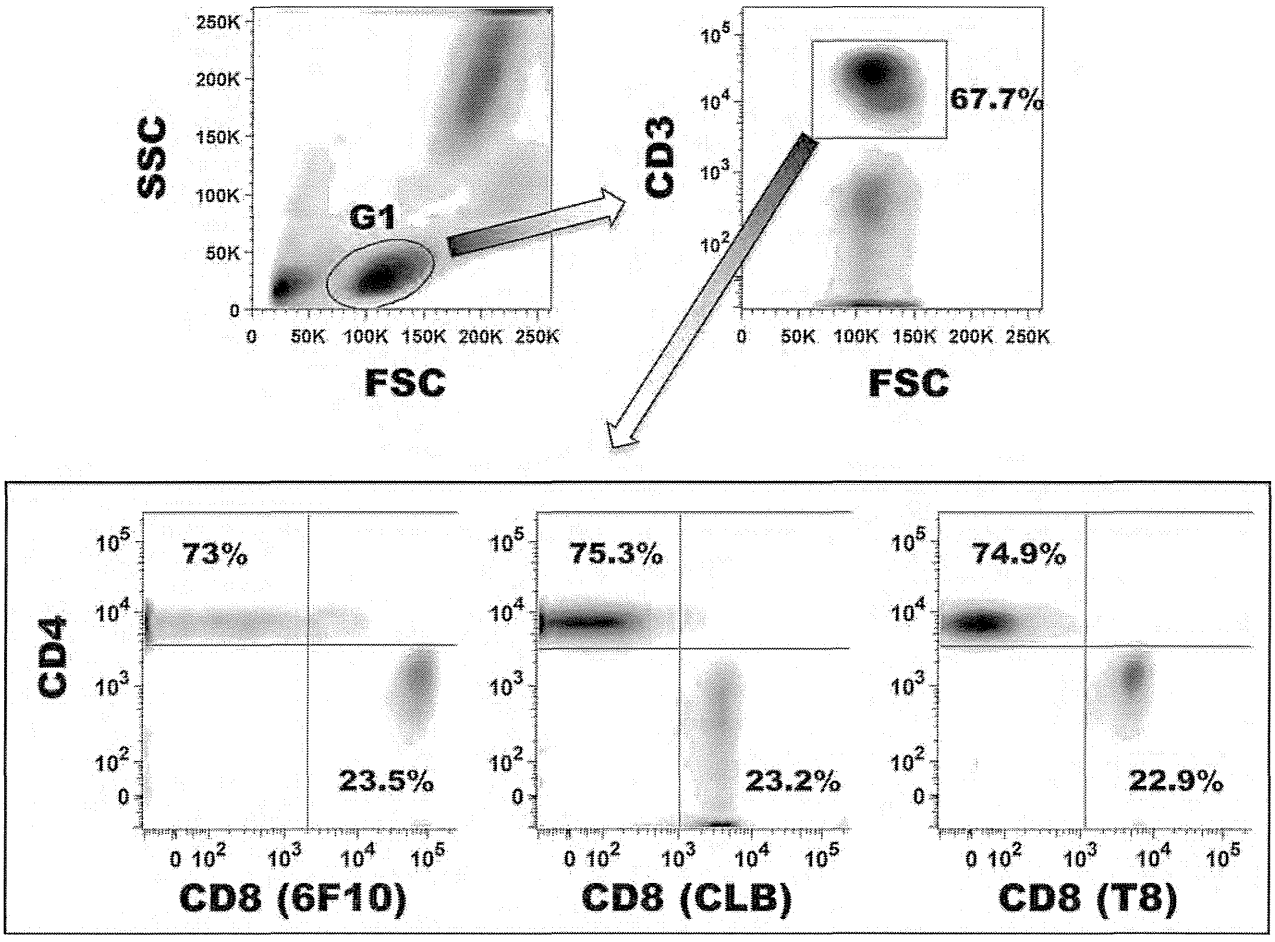

Fig. 1. Flow cytometric analyses of CD3, CD4 and CD8 expression on lymphocytes in marmosets. Fifty microliters of whole blood specimens from marmosets were stained with APC-Cy7-conjugated anti-CD3, PerCP-Cy5.5-conjugated anti-CD4 and APC-conjugated 6F10 mAbs or PE-conjugated CD8 (CLB or T8) mAb. Then, erythrocytes were lyzed and the stained cells were resuspended in the fix buffer. Representative results in a marmoset are shown. The G1 lymphocyte population was selected (left top panel) and a $CD3^+$ T cell subset was gated (right top panel). Fluorescence intensity for CD4 and CD8 in the T cell subset was depicted (lower panels).

three marmosets, weighing 357–457 g, were used. Common marmosets were caged individually at 27 ± 2 °C in 50 ± 10% humidity with a 12 h light–dark cycle (lighting from 7:00 to 19:00) in our facility. All animals were fed twice a day with a standard marmoset diet supplemented with fruit and mealworm. Water was given *ad libitum*.

2.2. Flow cytometry

Flow cytometry was performed as previously described with a slight modification [22]. A previously established mouse anti-marmoset CD8 mAb named 6F10 was used [7]. The 6F10 mAb was conjugated with allophycocyanin (APC) and by Zenon Mouse IgG labeling Kit (Molecular Probes) according to the manufacturer's instruction. Fifty microliters of whole blood from marmosets was stained with combinations of fluorescence-conjugated mAb: APC-Cy7-conjugated anti-CD3 (SP34-2: Becton Dickinson), PerCP-Cy5.5-conjugated anti-CD4 (L200: BD Pharmingen), PE-conjugated anti-CD8 (CLB-T8/4, 4H8 (CLB hereafter): Sanquin; RPA-T8 (T8 hereafter): Becton Dickinson) and FITC-conjugated anti-CD20 (H299: BECKMAN COULTER). Then, erythrocytes were lyzed with FACS lyzing solution (Becton Dickinson). After washing with a sample buffer containing phosphate-buffered saline (PBS) and 1% fetal calf serum (FCS), the labeled cells were resuspended in a fix buffer containing PBS and 1% formaldehyde. The expression of the immunolabeled molecules on the lymphocytes was analyzed with a FACSCanto II flow cytometer (Becton Dickinson). The data analysis was conducted using FlowJo software (Treestar, Inc.).

2.3. In vitro binding competition of anti-CD8 mAbs

Fifty microliters of whole blood from marmosets was treated with increasing amounts (1, 10, 100 ng) of the 6F10 mAb on ice for 30 min. After washing with the sample buffer, the cells were stained with fluorescence-conjugated mAbs against CD3, CD4, and CD8 on ice for 30 min. Then, erythrocytes were lyzed with FACS lyzing solution (Becton Dickinson). After washing with the sample buffer, the labeled cells were resuspended in the fix buffer. The fluorescence intensity of the cells were analyzed at is as described above.

2.4. In vivo depletion of $CD8^+$ T lymphocytes

In vivo depletion of the marmoset $CD8^+$ T lymphocytes was performed as previously described [19]. Briefly, the 6F10 or a control mAb (MOPC-21) was administrated subcutaneously to the subject at 10 mg/kg (body weight) followed by intravenous administration at 5 mg/kg in the saphenous vein at a rate of 20 ml/h using a syringe pump on days 3, 7, 10 after the primary administration. The kinetics for the percentages of $CD8^+$ and $CD4^+$ cells in a $CD3^+$ T cell subset as well as the percentages of $CD20^+$ B cells and $CD3^-CD20^-$ cells in the

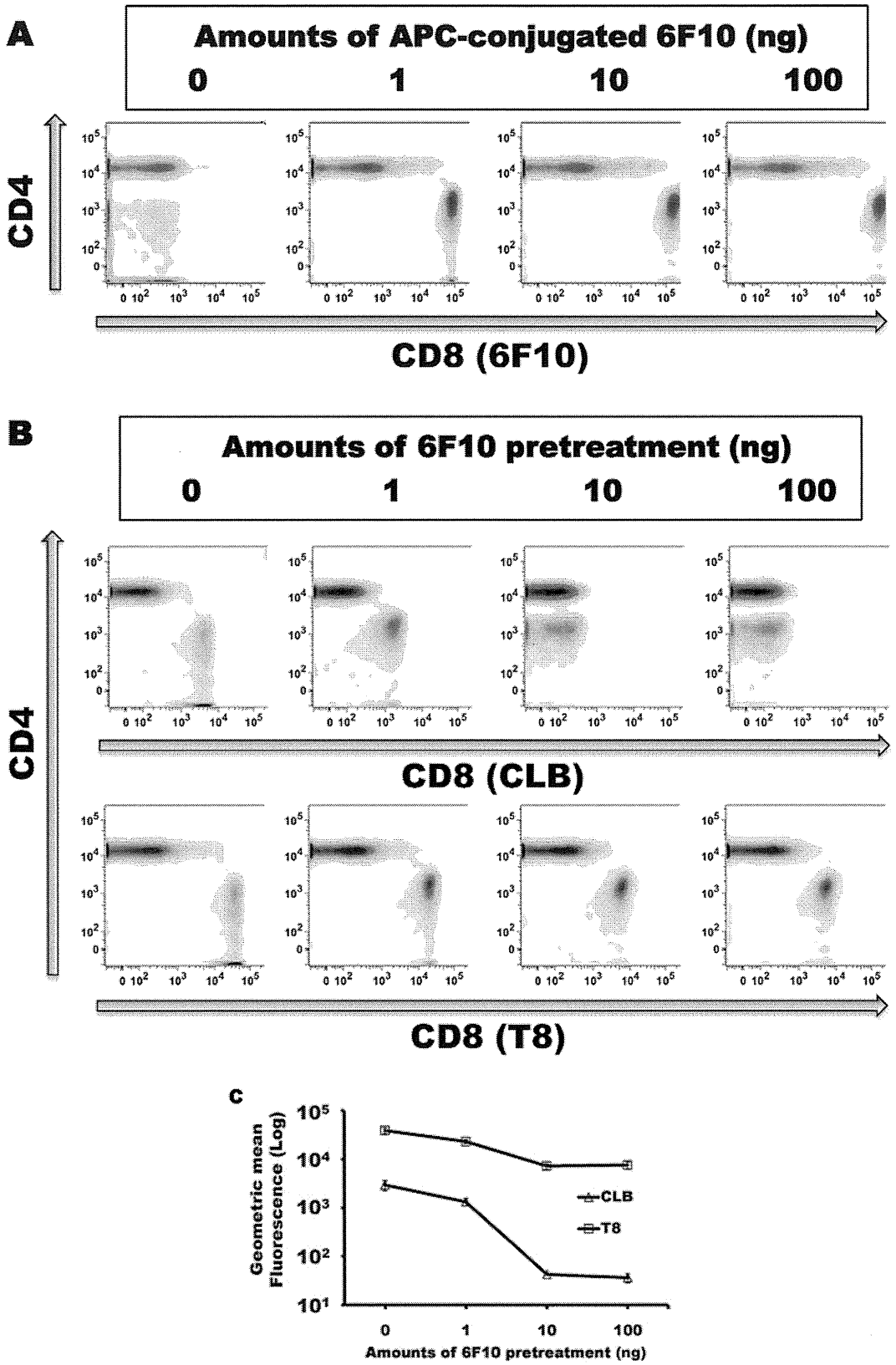

Fig. 2. Binding competition among anti-CD8 mAbs in marmoset CD8$^+$ T cells. (A) Fifty microliters of whole blood specimens from marmosets were stained with APC-Cy7-conjugated CD3 and PerCP-Cy5.5-conjugated CD4 mAbs and increasing amounts (1, 10, 100 ng) of APC-conjugated 6F10 mAb. Then, erythrocytes were lyzed and the stained cells were resuspended in the fix buffer. The fluorescence intensity for CD4$^+$ and CD8$^+$ cells in a CD3$^+$ T cell subset was shown. (B and C) Fifty microliters of whole blood specimens were pretreated with increasing amounts (1, 10, 100 ng) of 6F10 mAb, followed by staining with fluorescence-conjugated mAbs against CD3, CD4, and CD8 (CLB or T8). Fluorescence intensity of CD4$^+$ and CD8$^+$ cells in a CD3$^+$ T cell subset was shown (B) and the geometric mean fluorescence of CD8$^+$ T cells labeled by the CLB or T8 mAbs was indicated. We analyzed statistically whether geometric means were different in each antibody by using StatView software.

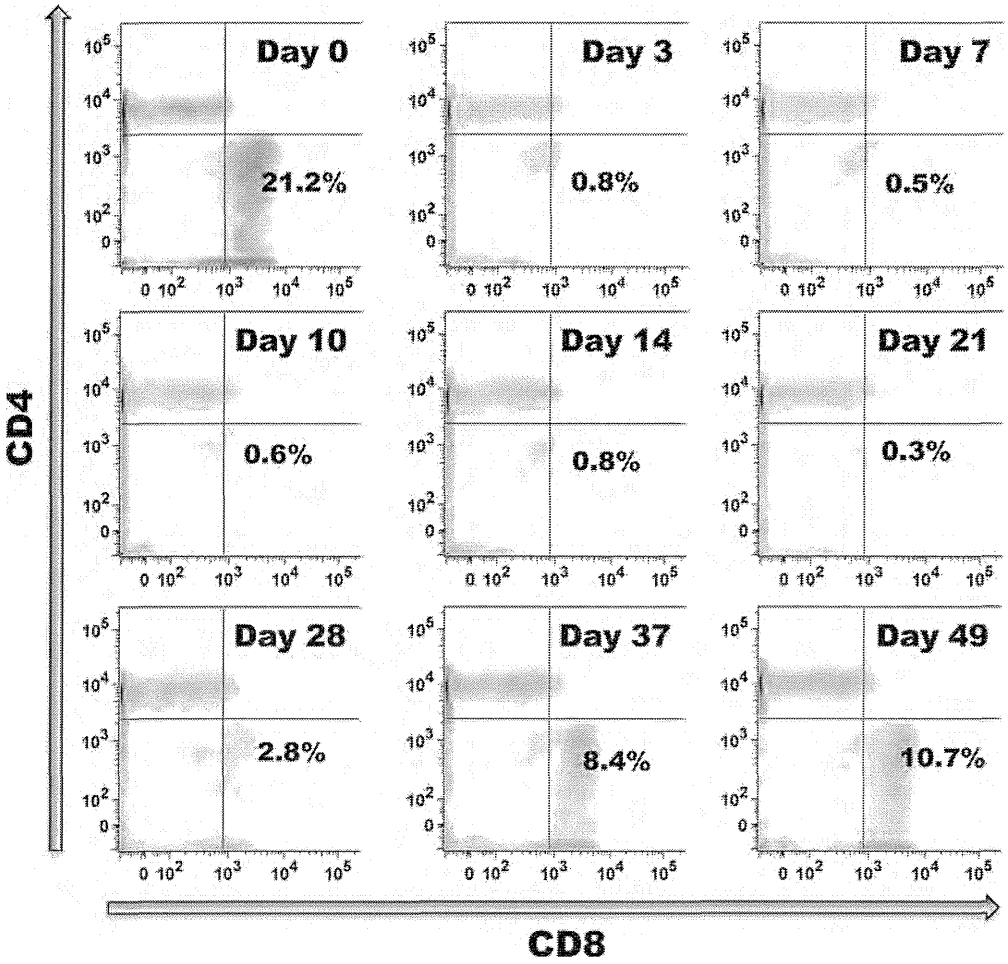

Fig. 3. *In vivo* depletion of CD8⁺ T cells by administration of a marmoset anti-CD8 mAb 6F10. Periodical kinetics for the fluorescence intensity of CD4⁺ and CD8⁺ cells in a CD3⁺ T cell subset of Cj175 administered subcutaneously with 10 mg/kg of the 6F10 mAb, followed by 5 mg/kg administration intravenously at days 3, 7, and 10 were shown.

total lymphocytes of each marmoset were periodically monitored during the observation period as indicated.

2.5. Statistical analyses

Statistical analyses of lymphocyte ratios were performed using Student's *t*-test and single-factor ANOVA, followed by Fisher's protected least-significant difference *post hoc* test by using StatView software (SAS Institute, NC, USA).

3. Results

3.1. Lymphocyte subsets in marmosets

We previously demonstrated that the 6F10 mAb specifically detected CD8⁺ T lymphocytes in marmosets by using flow cytometry as well as immunohistochemical and Western blot analyses [7]. Basic information regarding CD4/CD8 naïve and central/effector memory T cells and NK/NKT cells in marmosets was available from our recent report [13]. We compared the immunoreactivity of the 6F10 mAb with other commercially available CD8 mAbs in lymphocyte subsets of marmosets (Fig. 1). The gating strategy for profiling CD4⁺ and CD8⁺ T cells was shown in Fig. 1. The percentage of CD8⁺ T cells in a CD3⁺ T cell subset as detected by 6F10, CLB or T8 anti-CD8 mAb was comparable (23.5%, 23.2% and 22.9%, respectively). Notably, the 6F10 mAb poorly cross-reacted with tamarin and rhesus macaque CD8⁺ T cells while CLB and T8 mAbs did with both (data not shown). It is reasonable that the 6F10 mAb showed selected specificity to the marmoset CD8, considering that it was established by immunization with marmoset lymphocytes [7].

3.2. In vitro binding competition of anti-CD8 antibodies in CD8⁺ T cells of marmosets

We initially treated the marmoset lymphocytes with increasing amounts of APC-conjugated 6F10 together with fluorescence-labeled mAbs to CD3 and CD4. It was found that fluorescence intensity for APC on a CD3⁺ T cell subset was saturated by 10 ng or more of 6F10 mAb (Fig. 2A). We then sought to define whether the binding epitope of 6F10 mAb in the marmoset CD8 molecule was overlapped with the epitopes of T8 and CLB mAbs by a competition assay. It was found that fluorescence intensity in the CD3⁺ T cell subset treated with the labeled CLB mAb was drastically reduced by the pretreatment of 10 or 100 ng 6F10 (Fig. 2B and C). On the other hand, the 6F10 pretreatment scarcely influenced fluorescence intensity in the cells that reacted with the labeled T8 mAb, irrespective of the amounts of 6F10 (Fig. 2B and C). These results indicated that 6F10 competitively inhibited binding of CLB but not T8 mAbs to CD8, suggesting that the binding epitope for 6F10 was overlapped with that of CLB and was sterically apart from that of T8. In addition, T8 was likely to exhibit greater affinity than CLB to marmoset CD8 (Fig. 2B).

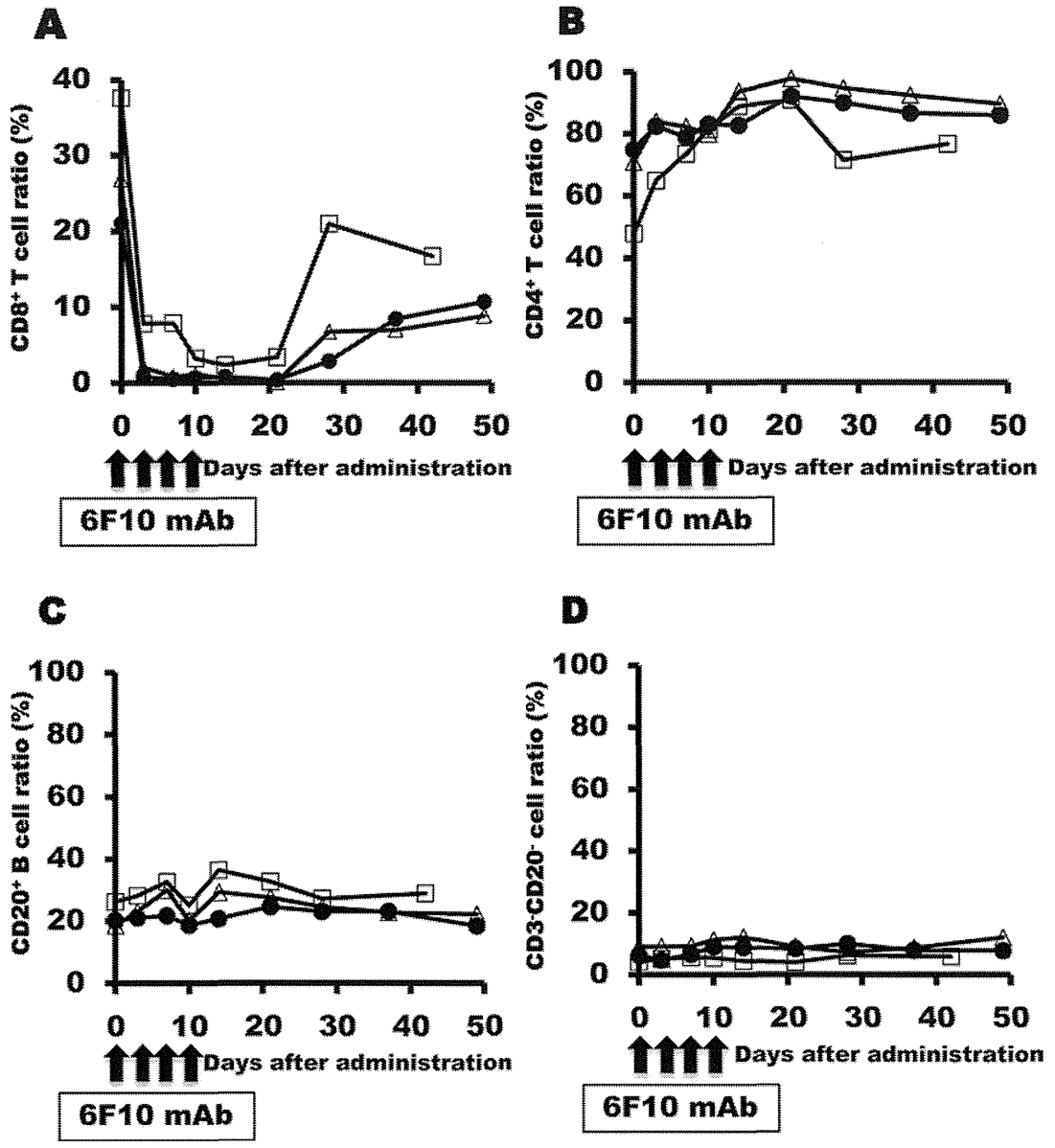

Fig. 4. The kinetics for the ratios of $CD8^+$ cells (A) and $CD4^+$ cells (B) in a $CD3^+$ T cell subset as well as $CD20^+$ B cells (C) and $CD3^-CD20^-$ cells (D) in total lymphocytes of each marmoset after the administration of the 6F10 mAb were shown.

3.3. In vivo depletion of $CD8^+$ T cells using an anti-marmoset CD8 mAb

We finally examined whether the administration of the 6F10 mAb could influence $CD8^+$ T lymphocytes *in vivo*. Three marmosets were subcutaneously administrated at 10 mg/kg followed by intravenous administration at 5 mg/kg on days 3, 7, 10 after the primary administration. The mAb-treated marmosets did not develop any clinical and hematological signs (data not shown). In order to detect $CD8^+$ T lymphocytes in the 6F10-treated marmosets, we employed T8 mAb, which was found to react with CD8 molecule in the presence of 6F10 as shown in Fig. 2. It was found that at 10 days after the mAb administration the $CD8^+$ T cells were almost completely depleted, followed by gradual recovery to a half of the initial levels at around 4–7 weeks later (Fig. 3). It is noteworthy that the treatment relatively increased in the proportion of $CD4^+$ T cells in compensation for the depletion of $CD8^+$ T cells, while the ratios of $CD20^+$ B cells and $CD3^-CD20^-$ cells were scarcely affected (Fig. 4). In addition, administration of a control antibody (MOPC-21) did not affect any lymphocyte subsets (data not shown). These results demonstrated that the 6F10 mAb was able to specifically deplete $CD8^+$ T cells in marmosets.

4. Discussion

In this study, we attempted to establish a technical basis for the study of $CD8^+$ T cells in marmosets. We assessed the effect of a 6F10 mAb administration *in vivo* and found that $CD8^+$ T cells were efficiently depleted in the blood of the treated monkeys for at least three weeks or longer and that in compensation for the depletion proportion of $CD4^+$ T cells were relatively increased without obvious influence on other lymphocyte subsets such as $CD20^+$ B cells and $CD3^-CD20^-$ cells. This is the first report showing the establishment of new methodology to deplete common marmoset $CD8^+$ T lymphocytes *in vivo*. Since demand for marmosets as non-human primate models for a variety of inflammatory and autoimmune diseases as well as infectious diseases has been increasing, our findings will provide new techniques to scientists who are eager to examine

the pivotal role of $CD8^+$ T lymphocytes *in vivo* in the onset of the human diseases.

We previously sought to examine the dynamics of cellular immune responses in the acute phase of dengue virus (DENV) infection in a novel marmoset model that we recently developed [12]. We found that the DENV infection in marmosets greatly induced early immune responses of CD4/CD8 central memory T cells, suggesting that the cellular immunity may be associated with the control of primary DENV infection [13]. Considering this, the present techniques to deplete $CD8^+$ T cells *in vivo* will provide a useful tool to further elucidate the functional role of $CD8^+$ T cells in the acute DENV infection.

Common marmosets are suitable for detailed observations of the movement of the extremities and cognitive functions, which approximate those of humans. Therefore, marmosets are highly useful as models of neurological diseases such as Parkinson's, MS and RA. Importantly, the marmoset models for analyzing Parkinson's disease and autoimmune diseases such as MS and RA have already been developed [8–10,23]. $CD8^+$ T cells have been implicated in the pathogenesis of autoimmune disorders including diseases of the central nervous system such as MS, encephalomyelitis and diabetes mellitus [24–26]. MS is an immune-mediated disease of the central nervous system leading to demyelination and axonal/neuronal loss. Accumulating evidence points to a key role for $CD8^+$ T cells in the disease; histopathological analyses and compelling observations from animal models indicate that cytotoxic $CD8^+$ T cells target neural cell populations with the potential of causing lesions consistent with MS [27]. RA is a systemic and chronic autoimmune disease characterized mainly by synovial inflammation leading to joint destruction and disability with a huge impact upon the quality of life and life expectancy. Several studies have demonstrated that $CD8^+$ T cells in RA have powerful cytotoxic ability and therefore exhibit the potential to enhance the disease [28]. Thus, our *in vivo* CD8 depletion technics will be valuable in further examining the role of $CD8^+$ T cells in these autoimmune diseases in the marmoset models.

Conflict of interest statement

None declared.

Acknowledgments

We would like to give special thanks to members of Corporation for Production and Research of Laboratory Primates and Center for Human Evolution Modeling Research, Primate Research Institute of Kyoto University for technical assistance. We also would like to give special thanks to Ms. Atsuko Owashi and Yumiko Hasegawa for technical assistance. This work was supported by grants from the Ministry of Health, Labor and Welfare of Japan and Ministry of Education, Culture, Sports, Science and Technology of Japan.

References

[1] Meuleman P, Leroux-Roels G. HCV animal models: a journey of more than 30 years. Viruses 2009;1:222–40.
[2] Zompi S, Harris E. Animal models of dengue virus infection. Viruses 2012;4:62–82.
[3] Gagneux P, Moore JJ, Varki A. The ethics of research on great apes. Nature 2005;437:27–9.
[4] Knight A. The beginning of the end for chimpanzee experiments? Philos Ethics Humanit Med 2008;3:16.
[5] Morimura N, Idani G, Matsuzawa T. The first chimpanzee sanctuary in Japan: an attempt to care for the "surplus" of biomedical research. Am J Primatol 2011;73:226–32.
[6] Brass V, Moradpour D, Blum HE. Hepatitis C virus infection: in vivo and in vitro models. J Viral Hepat 2007;14(Suppl. 1):64–7.
[7] Ito R, Maekawa S, Kawai K, Suemizu H, Suzuki S, Ishii H, et al. Novel monoclonal antibodies recognizing different subsets of lymphocytes from the common marmoset (*Callithrix jacchus*). Immunol Lett 2008;121:116–22.
[8] Ando K, Obayashi S, Nagai Y, Oh-Nishi A, Minamimoto T, Higuchi M, et al. PET analysis of dopaminergic neurodegeneration in relation to immobility in the MPTP-treated common marmoset, a model for Parkinson's disease. PLoS ONE 2012;7:e46371.
[9] Jagessar SA, Gran B, Heijmans N, Bauer J, Laman JD, t Hart BA, et al. Discrepant effects of human interferon-gamma on clinical and immunological disease parameters in a novel marmoset model for multiple sclerosis. J Neuroimmune Pharmacol 2012;7:253–65.
[10] Petersen F, Yu X. A novel preclinical model for rheumatoid arthritis research. Arthritis Res Ther 2010;12:148.
[11] Woollard DJ, Haqshenas G, Dong X, Pratt BF, Kent SJ, Gowans EJ. Virus-specific T-cell immunity correlates with control of GB virus B infection in marmosets. J Virol 2008;82:3054–60.
[12] Omatsu T, Moi ML, Hirayama T, Takasaki T, Nakamura S, Tajima S, et al. Common marmoset (*Callithrix jacchus*) as a primate model of dengue virus infection: development of high levels of viraemia and demonstration of protective immunity. J Gen Virol 2011;92:2272–80.
[13] Yoshida T, Omatsu T, Saito A, Katakai Y, Iwasaki Y, Kurosawa T, et al. Dynamics of cellular immune responses in the acute phase of dengue virus infection. Arch Virol 2013;158:1209–20.
[14] Omatsu T, Moi ML, Takasaki T, Nakamura S, Katakai Y, Tajima S, et al. Changes in hematological and serum biochemical parameters in common marmosets (*Callithrix jacchus*) after inoculation with dengue virus. J Med Primatol 2012;41:289–96.
[15] Barry AP, Silvestri G, Safrit JT, Sumpter B, Kozyr N, McClure HM, et al. Depletion of CD8+ cells in sooty mangabey monkeys naturally infected with simian immunodeficiency virus reveals limited role for immune control of virus replication in a natural host species. J Immunol 2007;178:8002–12.
[16] Castro BA, Homsy J, Lennette E, Murthy KK, Eichberg JW, Levy JA. HIV-1 expression in chimpanzees can be activated by CD8+ cell depletion or CMV infection. Clin Immunol Immunopathol 1992;65:227–33.
[17] Ramalingam RK, Meyer-Olson D, Shoukry NH, Bowen DG, Walker CM, Kalams SA. Kinetic analysis by real-time PCR of hepatitis C virus (HCV)-specific T cells in peripheral blood and liver after challenge with HCV. J Virol 2008;82:10487–92.
[18] Shoukry NH, Grakoui A, Houghton M, Chien DY, Ghrayeb J, Reimann KA, et al. Memory CD8+ T cells are required for protection from persistent hepatitis C virus infection. J Exp Med 2003;197:1645–55.
[19] Saito A, Nomaguchi M, Iijima S, Kuroishi A, Yoshida T, Lee YJ, et al. Improved capacity of a monkey-tropic HIV-1 derivative to replicate in cynomolgus monkeys with minimal modifications. Microbes Infect 2011;13:58–64.
[20] Jin X, Bauer DE, Tuttleton SE, Lewin S, Gettie A, Blanchard J, et al. Dramatic rise in plasma viremia after CD8(+) T cell depletion in simian immunodeficiency virus-infected macaques. J Exp Med 1999;189:991–8.
[21] Metzner KJ, Jin X, Lee FV, Gettie A, Bauer DE, Di Mascio M, et al. Effects of in vivo CD8(+) T cell depletion on virus replication in rhesus macaques immunized with a live, attenuated simian immunodeficiency virus vaccine. J Exp Med 2000;191:1921–31.
[22] Yoshida T, Saito A, Iwasaki Y, Iijima S, Kurosawa T, Katakai Y, et al. Characterization of natural killer cells in tamarins: a technical basis for studies of innate immunity. Front Microbiol 2010;1:128.
[23] Jagessar SA, Heijmans N, Bauer J, Biezer EL, Laman JD, Hellings N, et al. B-cell depletion abrogates T cell-mediated demyelination in an antibody-nondependent common marmoset experimental autoimmune encephalomyelitis model. J Neuropathol Exp Neurol 2012;71:716–28.
[24] Annibali V, Ristori G, Angelini DF, Serafini B, Mechelli R, Cannoni S, et al. CD161(high)CD8+ T cells bear pathogenetic potential in multiple sclerosis. Brain 2011;134:542–54.
[25] York NR, Mendoza JP, Ortega SB, Benagh A, Tyler AF, Firan M, et al. Immune regulatory CNS-reactive CD8+ T cells in experimental autoimmune encephalomyelitis. J Autoimmun 2010;35:33–44.
[26] Wang J, Ma Y, Knechtle SJ. Adenovirus-mediated gene transfer into rat cardiac allografts. Comparison of direct injection and perfusion. Transplantation 1996;61:1726–9.
[27] Saxena A, Martin-Blondel G, Mars LT, Liblau RS. Role of CD8 T cell subsets in the pathogenesis of multiple sclerosis. FEBS Lett 2011;585:3758–63.
[28] Carvalheiro H, da Silva JA, Souto-Carneiro MM. Potential roles for CD8(+) T cells in rheumatoid arthritis. Autoimmun Rev 2013;12:401–9.

Arch Virol (2013) 158:1209–1220
DOI 10.1007/s00705-013-1618-6

ORIGINAL ARTICLE

Dynamics of cellular immune responses in the acute phase of dengue virus infection

Tomoyuki Yoshida · Tsutomu Omatsu · Akatsuki Saito · Yuko Katakai · Yuki Iwasaki · Terue Kurosawa · Masataka Hamano · Atsunori Higashino · Shinichiro Nakamura · Tomohiko Takasaki · Yasuhiro Yasutomi · Ichiro Kurane · Hirofumi Akari

Received: 13 June 2012 / Accepted: 12 December 2012 / Published online: 5 February 2013

Abstract In this study, we examined the dynamics of cellular immune responses in the acute phase of dengue virus (DENV) infection in a marmoset model. Here, we found that DENV infection in marmosets greatly induced responses of CD4/CD8 central memory T and NKT cells. Interestingly, the strength of the immune response was greater in animals infected with a dengue fever strain than in those infected with a dengue hemorrhagic fever strain of DENV. In contrast, when animals were re-challenged with the same DENV strain used for primary infection, the neutralizing antibody induced appeared to play a critical role in sterilizing inhibition against viral replication, resulting in strong but delayed responses of CD4/CD8 central memory T and NKT cells. The results in this study may help to better understand the dynamics of cellular and humoral immune responses in the control of DENV infection.

T. Yoshida and T. Omatsu contributed equally to this study.

Electronic supplementary material The online version of this article (doi:10.1007/s00705-013-1618-6) contains supplementary material, which is available to authorized users.

T. Yoshida · Y. Iwasaki · T. Kurosawa · M. Hamano · Y. Yasutomi · H. Akari
Tsukuba Primate Research Center, National Institute of Biomedical Innovation, 1-1 Hachimandai, Tsukuba, Ibaraki 305-0843, Japan

T. Yoshida (✉) · A. Saito · A. Higashino · H. Akari (✉)
Center for Human Evolution Modeling Research, Primate Research Institute, Kyoto University, Inuyama, Aichi 484-8506, Japan
e-mail: yoshida.tomoyuki.4w@kyoto-u.ac.jp

H. Akari
e-mail: akari.hirofumi.5z@kyoto-u.ac.jp

Introduction

Dengue virus (DENV) causes the most prevalent arthropod-borne viral infections in the world [29]. Infection with one of the four serotypes of DENV can lead to dengue fever (DF) and sometimes to fatal dengue hemorrhagic fever (DHF) or dengue shock syndrome (DSS) [12]. The serious diseases are more likely to develop after secondary infection with a serotype of DENV that is different from that of the primary infection. Infection with DENV induces a high-titered neutralizing antibody response that can provide long-term immunity to the homologous DENV serotype, while the effect of the antibody on the heterologous serotypes is transient [22]. On the other hand, enhanced pathogenicity after secondary DENV infection appears to be explained by antibody-dependent enhancement (ADE). Mouse and monkey experiments have shown that sub-neutralizing levels of DENV-specific antibodies actually enhance infection [1, 6, 11]. Thus, the development of an effective tetravalent dengue vaccine is considered to be an important public-health priority. Recently, several DENV vaccine candidates have undergone clinical trials, and most of them target the induction of neutralizing antibodies [20].

T. Omatsu · T. Takasaki · I. Kurane
Department of Virology I, National Institute of Infectious Diseases, 1-23-1 Toyama, Shinjuku-ku, Tokyo 162-8640, Japan

Y. Katakai
Corporation for Production and Research of Laboratory Primates, 1-1 Hachimandai, Tsukuba, Ibaraki 305-0843, Japan

S. Nakamura
Research Center for Animal Life Science, Shiga University of Medical Science, Seta Tsukinowa-cho, Otsu, Shiga 520-2192, Japan

Research of the long-term immune response in humans has provided several interesting parallels to the data. It was reported that complete cross-protective immunity from heterologous challenge was induced in individuals 1–2 months after a primary DENV infection, with partial immunity present up to 9 months, resulting in a milder disease of shorter duration on reinfection, and that complete serotype-specific immunity against symptomatic dengue was observed up to 18 months postinfection [30]. Guzman and Sierra have previously recorded the long-term presence of both DENV-specific antibodies and T cells up to 20 years after natural infections [10, 31]. Of note, increased T cell activation is reportedly associated with severe dengue disease [7, 8]. Thus, the balance between humoral and cellular immunity may be important in the control of dengue diseases.

However, the details regarding the implication of humoral and cellular immunity in controlling DENV infection remain to be elucidated. Previously, passive transfer of either monoclonal or polyclonal antibodies was shown to protect against homologous DENV challenge [13, 15, 16]. It was also reported that neutralizing antibodies played a greater role than cytotoxic T lymphocyte (CTL) responses in heterologous protection against secondary DENV infection *in vivo* in IFN-$\alpha/\beta R^{-/-}$ and IFN$\gamma R^{-/-}$ mouse models [18]. Moreover, $CD4^+$ T cell depletion did not affect the DENV-specific IgG or IgM Ab titers or their neutralizing activity in the IFN$\gamma R^{-/-}$ mouse model [36]. On the other hand, there are several reports showing that cellular immunity rather than humoral immunity plays an important role in the clearance of DENV. For example, in adoptive transfer experiments, although cross-reactive DENV-1-specific $CD8^+$ T cells did not mediate protection against a lethal DENV-2 infection, adoptive transfer of $CD4^+$ T cells alone mediated protection and delayed mortality in IFN-$\alpha/\beta R^{-/-}$ and IFN$\gamma R^{-/-}$ mouse models [39]. It has also been demonstrated that $CD8^+$ T lymphocytes have a direct role in protection against DENV challenge in the IFN-$\alpha/\beta R^{-/-}$ mouse model of DENV infection by depleting $CD8^+$ T cells [35]. In addition, previous data from adoptive-transfer experiments in BALB/c mice showed that cross-reactive memory $CD8^+$ T cells were preferentially activated by the secondary DENV infection, resulting in augmented IFN-γ and tumor necrosis factor-α (TNF-α) responses, and this effect was serotype-dependent [2, 3]. Although it has previously been suggested that inducing neutralizing antibodies against DENV may play an important role in controlling DENV infection, CTLs are also proposed to contribute to clearance during primary DENV infection and to pathogenesis during secondary heterologous infection in the BALB/c mouse model [4].

Why did the mouse models of DENV infection show inconsistent results *in vivo*? One of the reasons could be that these results were obtained mainly from genetically manipulated mice such as IFN-$\alpha/\beta R^{-/-}$ and IFN$\gamma R^{-/-}$ mice. Moreover, these mice were inoculated with 10^9–10^{10} genome equivalents (GE) of DENV [27, 35, 36], which were likely in large excess compared with the 10^4-10^5 GE of DENV injected into humans by a mosquito [19]. In addition, the efficiency of DENV replication in wild mice *in vivo* is very low compared to that in humans [35].

Recently, novel non-human primate models of DENV infection using rhesus macaques as well as marmosets and tamarins have been developed [24–26, 38]. An intravenous challenge of rhesus macaques with a high dose of virus inoculum (1×10^7 GE) of DENV-2 resulted in readily visible hemorrhaging, which is one of the cardinal symptoms of human DHF [26]. It was also shown that the cellular immune response was activated due to expression of IFN-γ, TNF-α, and macrophage inflammatory protein-1 β in $CD4^+$ and $CD8^+$ T cells during primary DENV infection in rhesus macaques [20]. On the other hand, in the marmoset model of DENV infection, we observed high levels of viremia (10^5–10^7 GE/ml) after subcutaneous inoculation with 10^4–10^5 plaque-forming units (PFU) of DENV-2. Moreover, we demonstrated that DENV-specific IgM and IgG were consistently detected and that the DENV-2 genome was not detected in any of these marmosets inoculated with the same DENV-2 strain used in the primary infection [24]. It is notable that while neutralizing antibody titers were at levels of 1:20-1:80 before the re-challenge inoculation, the titers increased up to 1:160-1:640 after the re-challenge inoculation [24]. These results suggested that the secondary infection with DENV-2 induced a protective humoral immunity to DENV-2 and that DENV-infected marmoset models may be useful in order to analyze the relationship between DENV replication and the dynamics of adaptive immune responses *in vivo*.

Taking these findings into consideration, we investigated the dynamics of cellular immunity in response to primary and secondary DENV infection in the marmoset model.

Materials and methods

Animals

All animal studies were conducted in accordance with protocols of experimental procedures that were approved by the Animal Welfare and Animal Care Committee of the National Institute of Infectious Diseases, Japan, and the National Institute of Biomedical Innovation, Japan. A total of six male marmosets, weighing 258–512 g, were used. Common marmosets were purchased from Clea Japan Inc.

(Tokyo, Japan) and caged singly at 27 ± 2 °C in 50 ± 10 % humidity with a 12-h light-dark cycle (lighting from 7:00 to 19:00) at Tsukuba Primate Research Center, National Institute of Biomedical Innovation, Tsukuba, Japan. Animals were fed twice a day with a standard marmoset diet (CMS-1M, CLEA Japan) supplemented with fruit, eggs and milk. Water was given ad libitum. The animals were in healthy condition and confirmed to be negative for anti-dengue-virus antibodies before inoculation with dengue virus [24].

Cells

Cell culture was performed as described previously [24]. Vero cells were cultured in minimum essential medium (MEM, Sigma) with 10 % heat-inactivated fetal bovine serum (FBS, GIBCO) and 1 % non-essential amino acid (NEAA, Sigma) at 37 °C in 5 % CO_2. C6/36 cells were cultured in MEM with 10 % FBS and 1 % NEAA at 28 °C in 5 % CO_2.

Virus

DENV type 2 (DENV-2) strain DHF0663 (accession no. AB189122) and strain D2/Hu/Maldives/77/2008NIID (Mal/77/08) were used for inoculation studies. The DENV-2, DHF0663 strain was isolated from a DHF case in Indonesia. The DENV-2 Mal/77/08 strain was isolated from imported DF cases from the Maldives. For all DENV strains, isolated clinical samples were propagated in C6/36 cells and were used within four passages on C6/36 cells. Culture supernatant from infected C6/36 cells was

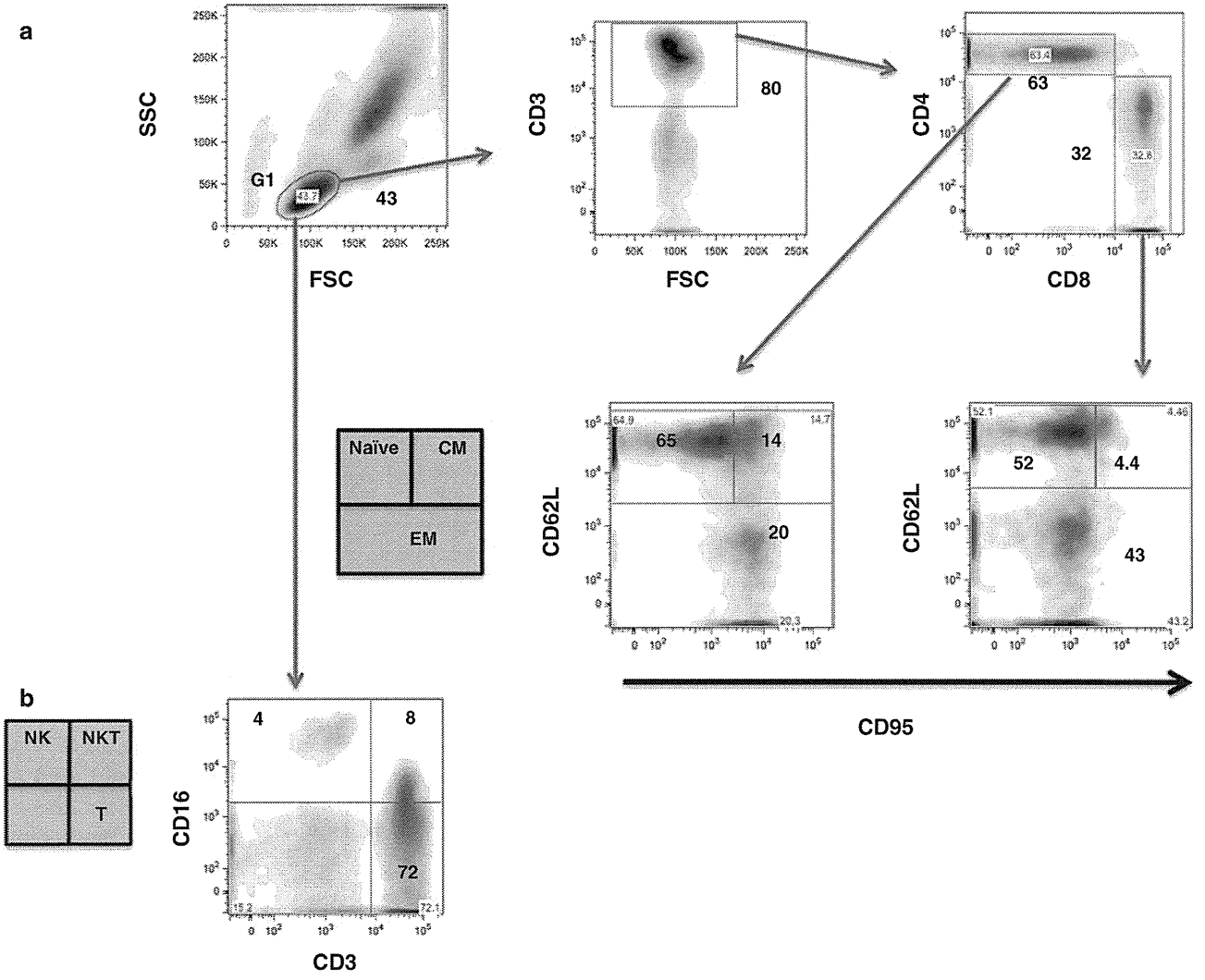

Fig. 1 Flow cytometric analysis of naïve, central/effector memory T cells and NK/NKT cells in marmosets. (**a**) Gating strategy to indentify CD4 and CD8 T, NK and NKT cells. The G1 population was selected and analyzed for CD4 and CD8 T, NK and NKT cells. (**a**) Profiling of naïve, central memory, and effector memory CD4 and CD8 T cells in total CD4 and CD8 T cells. (**b**) Profiling of NK and NKT cells in total lymphocytes. Results shown are representative of three healthy marmosets used in this study

centrifuged at 3,000 rpm for 5 min to remove cell debris and then stored at −80 °C until use.

Infection of the marmosets with DENV

In the challenge experiments, profiling of the key adaptive and innate immune cells in the marmosets after infection with DENV-2 was done. For primary DENV infection, four marmosets were inoculated subcutaneously in the back with either 1.9×10^5 PFU of the DENV-2 Mal/77/08 strain (Cj08-007, Cj07-011) or 1.8×10^4 PFU of the DHF0663 strain (Cj07-006, Cj07-008) [24]. In the case of the DENV re-challenge experiment, two marmosets initially inoculated with 1.8×10^5 PFU of the DHF0663 strain were re-inoculated 33 weeks after the primary challenge with 1.8×10^5 PFU of the same strain (Cj07-007, Cj07-014) [24]. Blood samples were collected on days 0, 1, 3, 7, 14, and 21 after inoculation and were used for virus titration and flow cytometric analysis. Inoculation with DENV and blood drawing were performed under anesthesia with 5 mg/kg of ketamine hydrochloride. Day 0 was defined as the day of virus inoculation. The viral loads in marmosets obtained in a previous study are shown in Supplementary Figure 1 [24].

Flow cytometry

Flow cytometry was performed as described previously [37]. Fifty microliters of whole blood from marmosets was stained with combinations of fluorescence-conjugated monoclonal antibodies; anti-CD3 (SP34-2; Becton Dickinson), anti-CD4 (L200; BD Pharmingen), anti-CD8 (CLB-T8/4H8; Sanquin), anti-CD16 (3G8; BD Pharmingen), anti-CD95 (DX2; BD Pharmingen), and anti-CD62L (145/15; Miltenyi Biotec). Then, erythrocytes were lysed with FACS lysing solution (Becton Dickinson). After washing with a sample buffer containing phosphate-buffered saline (PBS) and 1 % FBS, the labeled cells were resuspended in a fix buffer containing PBS and 1 % formaldehyde. The expression of these markers on the lymphocytes was analyzed using a FACSCanto II flow cytometer (Becton Dickinson). The data analysis was conducted using FlowJo software (Treestar, Inc.). Results are shown as mean ± standard deviation (SD) for the marmosets used in this study.

Table 1 Subpopulation ratios of lymphocytes in marmosets

Subpopulation name	Subpopulation ratios (Mean ± SD: %)
$CD3^+$	75.7 ± 6.4
$CD3^+CD4^+$	65.4 ± 6.8
$CD3^+CD4^+CD62L^+CD95^-$ (CD4 T_N)	65.9 ± 3.7
$CD3^+CD4^+CD62L^+CD95^+$(CD4 T_{CM})	16.4 ± 2.9
$CD3^+CD4^+CD62LCD95^{\pm}$ (CD4 T_{EM})	19.5 ± 2.5
$CD3^+CD8^+$	29.0 ± 8.0
$CD3^+CD8^+CD62L^+CD95^-$ (CD8 T_N)	66.7 ± 10.2
$CD3^+CD8^+CD62L^+CD95^+$(CD8 T_{CM})	4.7 ± 3.6
$CD3^+CD8^+CD62LCD95^{\pm}$ (CD8 T_{EM})	28.8 ± 14.8
CD3CD16 + (NK)	4.2 ± 2.6
$CD3^+CD16^+$ (NKT)	5.1 ± 3.4

SD: Standard deviation

Results shown are mean ± SD from 3 healthy marmosets

Results

Naïve central/effector memory T cells and NK/NKT cells in marmosets

Basic information regarding CD4/CD8 naïve and central/effector memory T cells and NK/NKT cells in common marmosets was unavailable. Thus, we examined the immunophenotypes of lymphocyte subsets in the marmosets (Fig. 1). The gating strategy for profiling the CD4 and CD8 T cells in the marmosets by FACS is shown in Fig. 1a. Human T cells are classically divided into three functional subsets based on their cell-surface expression of CD62L and CD95, i.e., $CD62L^+CD95^-$ naive T cells (T_N), $CD62L^+CD95^+$ central memory T cells (T_{CM}), and $CD62L^-CD95^{\pm}$ effector memory T cells (T_{EM}) [9, 21, 28]. In this study, $CD4^+$ and $CD8^+$ T_N, T_{CM}, and T_{EM} subpopulations were defined as $CD62L^+CD95^-$, $CD62L^+CD95^+$, and $CD62L^-CD95^{\pm}$, respectively (Fig. 1a and Table 1). The average ratio of $CD3^+$ T lymphocytes in the total lymphocytes of three marmosets was found to be 75.7 ± 6.4 %. The average ratio of $CD4^+$ T cells in the $CD3^+$ subset was 65.4 ± 6.8 %. The average ratios of $CD4^+$ T_N, T_{CM}, and T_{EM} cells were 65.9 ± 3.7 %, 16.4 ± 2.9 %, 19.5 ± 2.5 %, respectively. The average ratio of $CD8^+$ T cells in the $CD3^+$ subset was 29.0 ± 8.0 %. The average ratios of $CD8^+$ T_N, T_{CM}, and T_{EM} cells were 66.7 ± 10.2 %, 4.7 ± 3.6 %, 28.8 ± 14.8 %, respectively.

We recently characterized a $CD16^+$ major NK cell subset in tamarins and compared NK activity in tamarins with or without DENV infection [37, 38]. In terms of NKT cells, NK1.1 (CD161) and CD1d are generally used as markers of NKT cells [32]. However, these anti-human NK1.1 and CD1d antibodies are unlikely to cross-react with the NKT cells of the marmosets. Thus, we defined NKT cells as a population expressing both CD3 and CD16 as reported previously [14, 17]. The NK and NKT cell subsets were determined to be $CD3^-CD16^+$ and $CD3^+CD16^+$ lymphocytes in the marmosets. The average ratios of NK and NKT cell subsets in the lymphocytes were 4.2 ± 2.6 % and 5.1 ± 3.4 %, respectively (Table 1). We observed that the proportions of the major lymphocyte

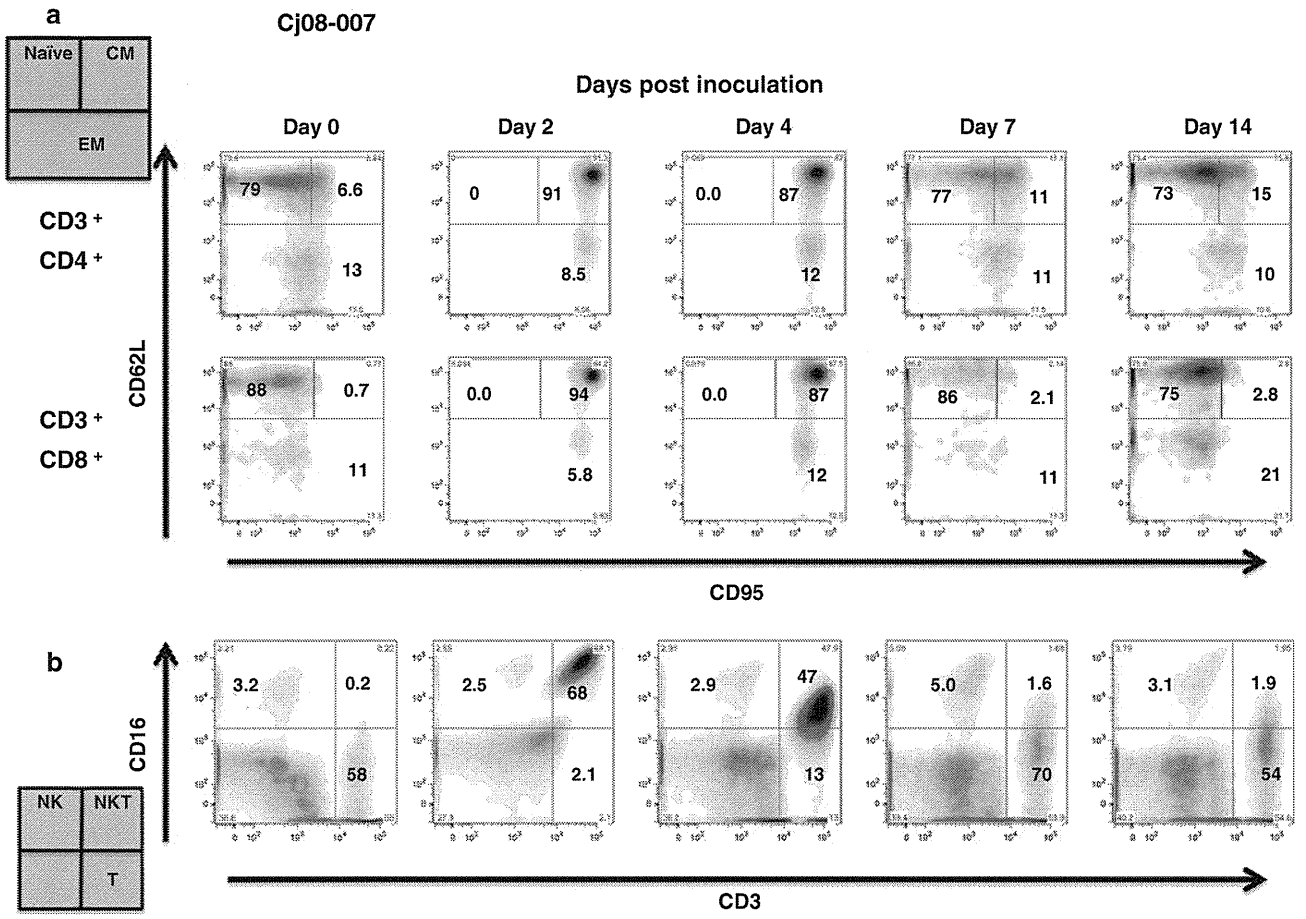

Fig. 2 Profiling of CD4 and CD8 T, NK and NKT cells in marmosets with primary infection with the DENV-2 Mal/77/08 strain. For primary DENV infection, two marmosets were inoculated subcutaneously in the back with 1.9×10^5 PFU of the DENV-2 Mal/77/08 strain. (**a**) Profiling of naïve, central memory, and effector memory CD4 and CD8 T cells in total CD4 and CD8 T cells. (**b**) Profiling of NK and NKT cells in total lymphocytes. (**a-b**) Cj08-007

subsets in the marmosets were similar to those in cynomolgus monkeys and tamarins [37, 38].

Profiling of CD4 and CD8 T, NK and NKT cells in marmosets after primary infection with DENV-2 (Mal/77/08 strain)

We investigated the cellular immune responses against DENV-2 DF strain (Mal/77/08) in marmosets. Dengue vRNA was detected in plasma samples from two marmosets on day 2 postinfection (Supplementary Fig. 1a). For the two marmosets (Cj08-007, Cj07-011), the plasma levels of vRNA reached their peaks at 9.6×10^6 and 7.0×10^6 GE/ml, respectively, on day 4 postinfection. Plasma vRNA was detected in both marmosets on days 2, 4, and 7. We then examined the profiles and frequencies of the CD4 and CD8 T, NK and NKT cells in the infected marmosets (Figs. 2–3 and Table 2). $CD4^+$ T_{CM} cells drastically increased to 88.7 ± 2.8 % from 13 ± 0.4 % between day 0 and day 2 post-inoculation (Table 2). Reciprocally, $CD4^+$ T_N cells decreased to 1.6 ± 3.3 % from 74.1 ± 0.9 % at the same time. $CD4^+$ T_{EM} cells maintained the initial levels throughout the observation period. $CD8^+$ T_{CM} cells increased to 91.9 ± 5.5 % from 2.1 ± 0.8 % between day 0 day 2 post-inoculation, and reciprocally, $CD8^+$ T_N cells decreased to 2.5 ± 4.7 % from 89.9 ± 2.5 % at the same time. In addition, NK cells maintained their initial levels throughout the observation period. However, NKT cells drastically increased to 52.6 ± 17 % from 0.2 ± 0.0 % between day 0 and day 2 post-inoculation. These results suggest that CD4/CD8 T and NKT cells may efficiently respond to the Mal/77/08 strain of DENV.

Profiling of CD4 and CD8 T, NK and NKT cells in the marmosets after primary infection with DENV-2 (DHF0663 strain)

Next, we investigated cellular immune responses against another DENV-2 DHF strain (DHF0663) in marmosets.

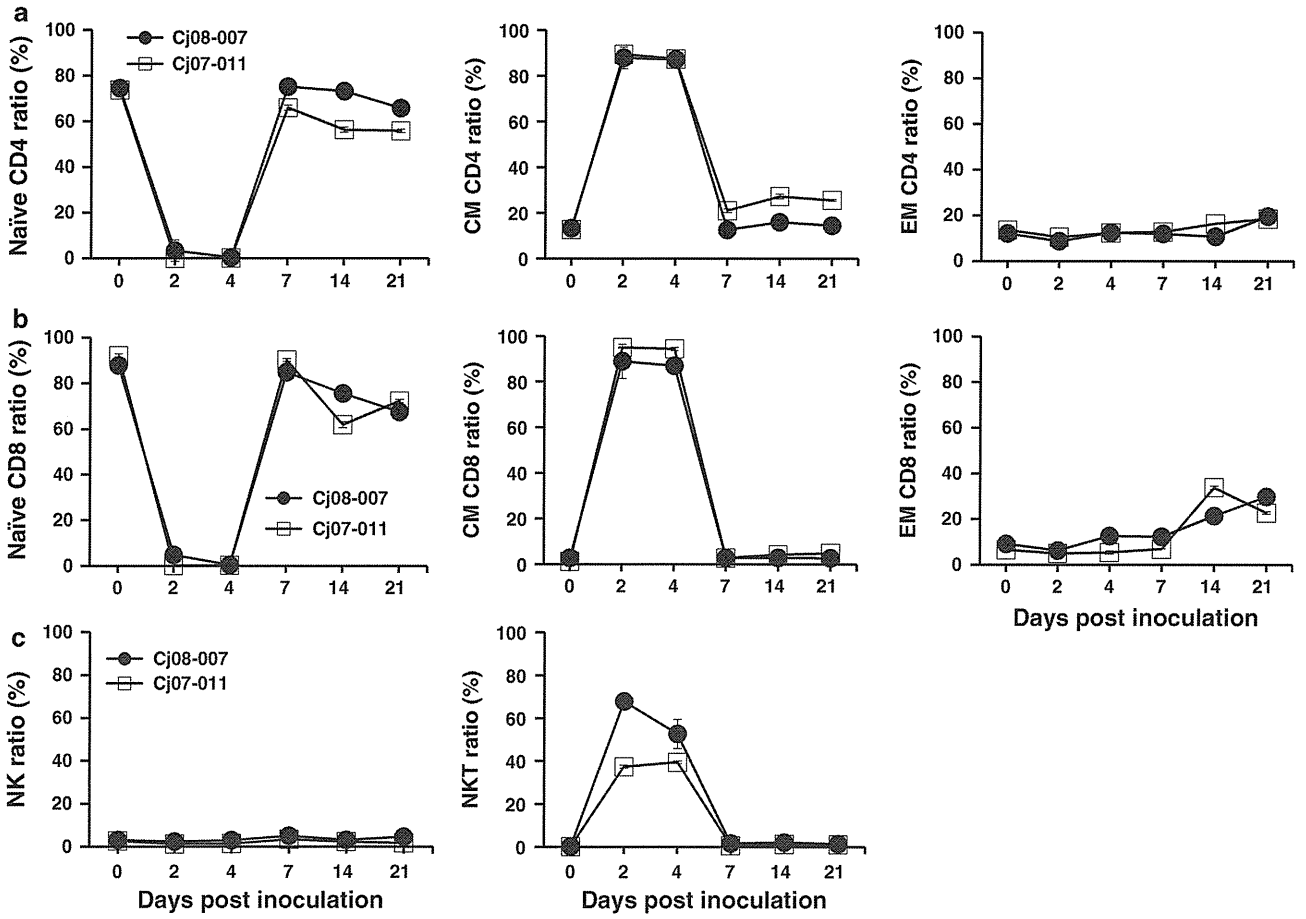

Fig. 3 Frequency of CD4 and CD8 T, NK and NKT cells in marmosets with primary infection with the DENV-2 Mal/77/08 strain. For primary DENV infection, two marmosets were inoculated subcutaneously in the back with 1.9×10^5 PFU of the DENV-2 Mal/77/08 strain. (**a**) Ratios of naïve, central memory, and effector memory CD4 T cells in total CD4 T cells. (**b**) Ratios of naïve, central memory, and effector memory CD8 T cells in total CD8 T cells. (**c**) Ratios of NK and NKT cells in total lymphocytes. (**a**-**c**) Cj08-007, Cj07-011

Table 2 Subpopulation ratios of lymphocytes in marmosets during primary DENV infection (Mal/77/08)

Subpopulation name		Subpopulation ratio (Mean ± SD: %)					
		Days after inoculation					
		Day 0	Day 2	Day 4	Day 7	Day 14	Day 21
$CD3^+CD4^+CD62L^+CD95''$	(CD4 T_N)	74.1 ± 0.9	1.6 ± 3.3	0.2 ± 0.3	70.5 ± 5.5	64.8 ± 9.7	60.8 ± 5.9
$CD3^+CD4^+CD62L^+CD95^+$	(CD4 T_{CM})	13 ± 0.4	88.7 ± 2.8	87.4 ± 0.2	16.8 ± 5.0	21.6 ± 6.5	20 ± 6.4
$CD3^+CD4^+CD62LCD95^{\pm}$	(CD4 T_{EN})	12.8 ± 0.9	9.5 ± 1.0	12.3 ± 0.4	12.3 ± 0.5	134 ± 3.2	189 ± 1.4
$CD3^+CD8^+CD62L^+CD95^-$	(CD8 T_N)	89.9 ± 2.5	2.5 ± 4.7	0.3 ± 0.3	87.5 ± 3.3	68.7 ± 79	69.8 ± 3.1
$CD3^+CD8^+CD62L^+CD95^+$	(CD8 T_{CM})	2.1 ± 0.8	91.9 ± 5.5	90.6 ± 4.2	2.8 ± 0.5	3.5 ± 08	3.8 ± 1.2
$CD3^+CD8^+CD62LCD95^{\pm}$	(CD8 T_{EN})	7.8 ± 1.6	5.6 ± 0.8	9.0 ± 4.1	9.5 ± 3.1	27.6 ± 72	26.3 ± 4.3
$CD3^-CD16+$	(NK)	2.9 ± 0.2	1.8 ± 0.6	2.2 ± 0.9	4.2 ± 0.9	2.8 ± 04	3.2 ± 1.7
$CD3^+CD16^+$	(NKT)	0.2 ± 0.0	52.6 ± 17	46.1 ± 8.5	1.1 ± 05	1.7 ± 05	1.2 ± 0.2

SD: Standard deviation

Results shown are mean ± SD from two marmosets as shown in Figure 3

Dengue vRNA was detected in plasma samples from the marmosets on day 2 post-infection ([24], Supplementary Fig. 1b). For the two marmosets (Cj07-006, Cj07-008), the plasma vRNA levels were found to be 3.4×10^5 and 3.8×10^5 GE/ml on day 2 and 2.0×10^6 and 9.4×10^5 GE/ml, respectively, at the peak on day 4 post-infection and became undetectable by day 14. Thus, we examined the profiles and frequencies of the $CD4^+$ and $CD8^+$ T, NK and NKT cells in these DENV-infected marmosets (Fig. 4–5 and Table 3). It was found that on day 7 post-inoculation, $CD4^+$ and $CD8^+$ T_N cells decreased, and in contrast, the T_{CM} populations increased in both marmosets; however, the changes in proportion were much less pronounced than in the case of the marmosets infected with the DF strain. We observed no consistent tendency in the kinetics of $CD4^+$ and $CD8^+$ T_{EM} cells nor in NK and NKT cells. These results suggest that the strength of T cell responses may be dependent on the strain of DENV.

Profiling of CD4 and CD8 T, NK and NKT cells in marmosets re-challenged with a DENV-2 strain

In order to examine the cellular immune responses against re-challenge with a DENV-2 DHF strain in the marmoset model, marmosets were infected twice with the same DENV-2 strain (DHF0663) with an interval of 33 weeks after the primary infection. The results showed that vRNA and NS1 antigens were not detected in plasma and that the neutralizing antibody titer was obviously increased after the secondary infection. The data indicated that the primary infection induced protective immunity, including a neutralizing antibody response to re-challenge with the same DENV strain ([24]; Supplementary Fig. 1c). We also investigated the profiles of the CD4 and CD8 T, NK and NKT cells in the marmosets (Cj07-007, Cj07-014) that were re-challenged with the same DENV-2 strain (DHF0663) (Figs. 6–7). $CD4^+$ T_{CM} cells drastically increased on day 14 post-inoculation. On the other hand,

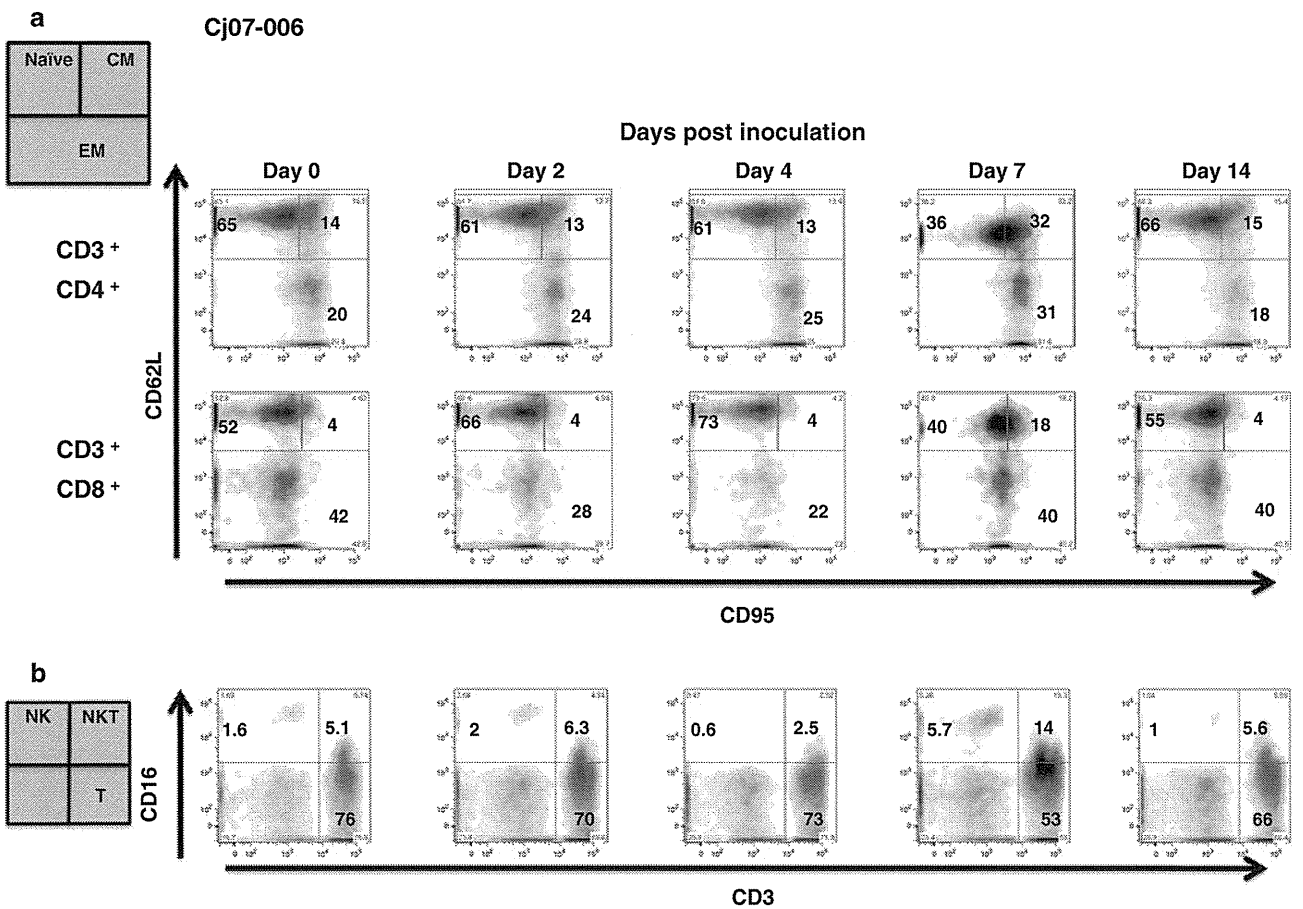

Fig. 4 Profiling of CD4 and CD8 T, NK and NKT cells in marmosets with primary infection with the DENV-2 DHF0663 strain. For primary DENV infection, two marmosets were inoculated subcutaneously in the back with 1.8×10^4 PFU of the DENV-2 DHF0663 strain. (**a**) Profiling of naïve, central memory, and effector memory CD4 and CD8 T cells in total CD4 and CD8 T cells. (**b**) Profiling of NK and NKT cells in total lymphocytes. (**a-b**) Cj07-006

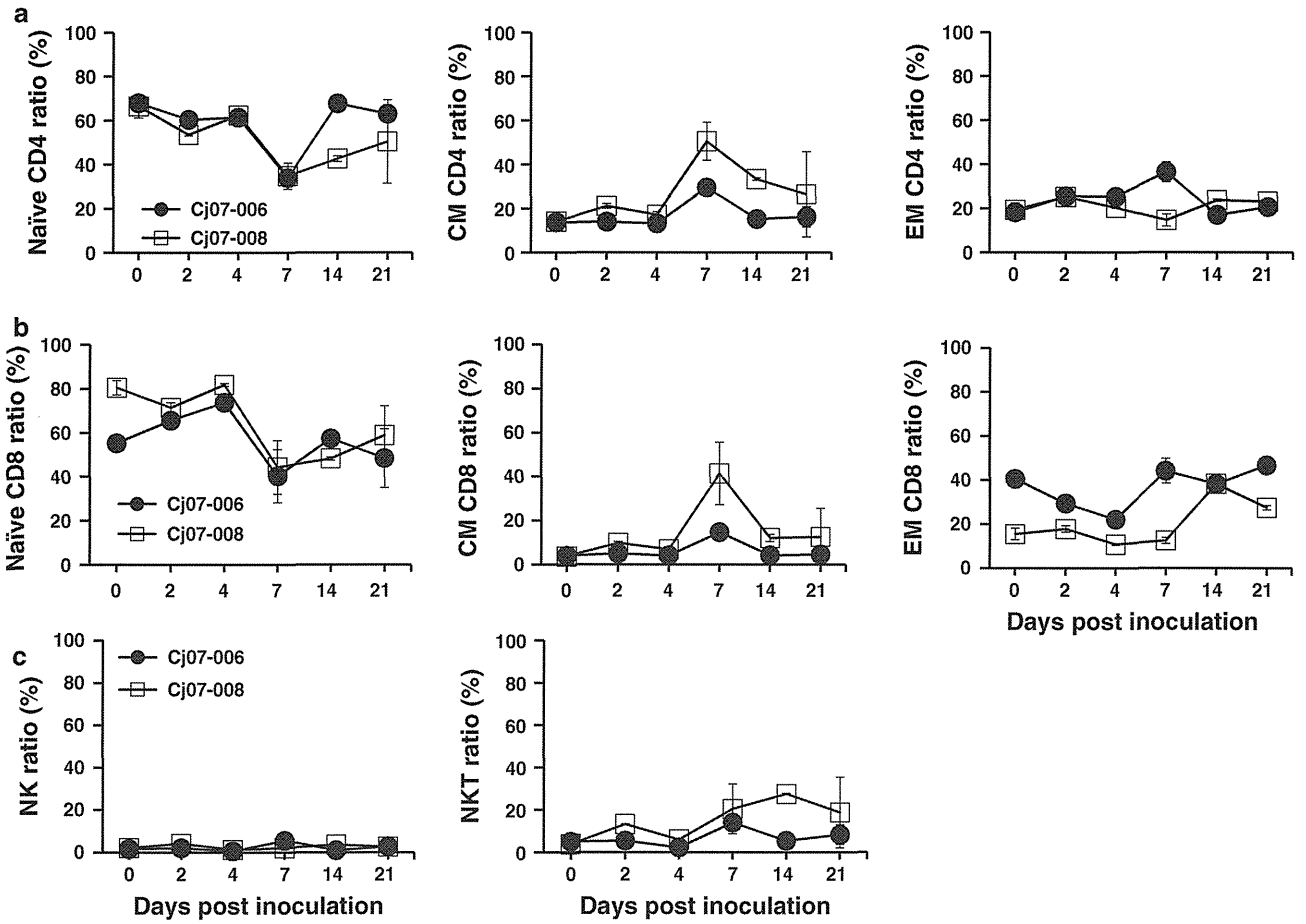

Fig. 5 Frequency of CD4 and CD8 T, NK and NKT cells in marmosets with primary infection with the DENV-2 DHF0663 strain. For primary DENV infection, two marmosets were inoculated subcutaneously in the back with 1.8×10^4 PFU of the DENV-2 DHF0663 strain. (**a**) Ratios of naïve, central memory, and effector memory CD4 T cells in total CD4 T cells. (**b**) Ratios of naïve, central memory, and effector memory CD8 T cells in total CD8 T cells. (**c**) Ratios of NK and NKT cells in total lymphocytes. (**a-c**) Cj07-006, Cj07-008

Table 3 Subpopulation ratios of lymphocytes in marmosets during primary DENV infection (DHF0663)

Subpopulation name		Subpopulation ratios (Mean ± SD: %)					
		Days after inoculation					
		Day 0	Day 2	Day 4	Day 7	Day1 4	Day 21
$CD3^+CD4^+CD62L^+CD95^-$	($CD4\ T_N$)	67.3 ± 3.6	57.0 ± 4.0	61.9 ± 0.9	34.4 ± 3.6	55.2 ± 14	56.7 ± 13
$CD3^+CD4^+CD62L^+CD95^+$	($CD4T_{CM}$)	13.9 ± 1.3	17.5 ± 4.1	15.2 ± 2.5	40.0 ± 13	33.8 ± 10	21.3 ± 12
$CD3^+CD8^+CD62L^-CD95^{\pm}$	($CD4\ T_{EM}$)	18.8 ± 2.2	25.3 ± 0.9	22.8 ± 2.9	25.6 ± 13	20.3 ± 4.0	21.8 ± 1.5
$CD3^+CD8^+CD62L^+CD95^-$	($CDS\ T_N$)	67.8 ± 14	68.4 ± 3.7	77.7 ± 4.6	42.2 ± 7.4	52.7 ± 5.5	53.5 ± 9.8
$CD3^+CD8^+CD62L^+CD95^-$	($CDS\ T_{CM}$)	3.9 ± 0.6	7.4 ± 2.8	5.5 ± 1.6	28 ± 17	8.1 ± 4.6	8.6 ± 8.9
$CD3^+CD8^+CD62L^-CD95^{\pm}$	($CDS\ T_{EM}$)	28 ± 14	23.5 ± 6.7	16.4 ± 6.5	28.3 ± 18	38.2 ± 1.9	37.0 ± 11
$CD3^-CD16^+$	(NK)	4.7 ± 1.0	4.2 ± 1.9	2.0 ± 1.1	6.3 ± 2.3	5.1 ± 2.2	7.3 ± 1.2
$CD3^+CD16^+$	(NKT)	7.8 ± 1.0	9.3 ± 4.5	5.9 ± 2.6	22.6 ± 8.4	20.6 ± 10	17.3 ± 10

SD: Standard deviation

Results shown are mean ± SD from 2 marmosets as shown in Figure 5

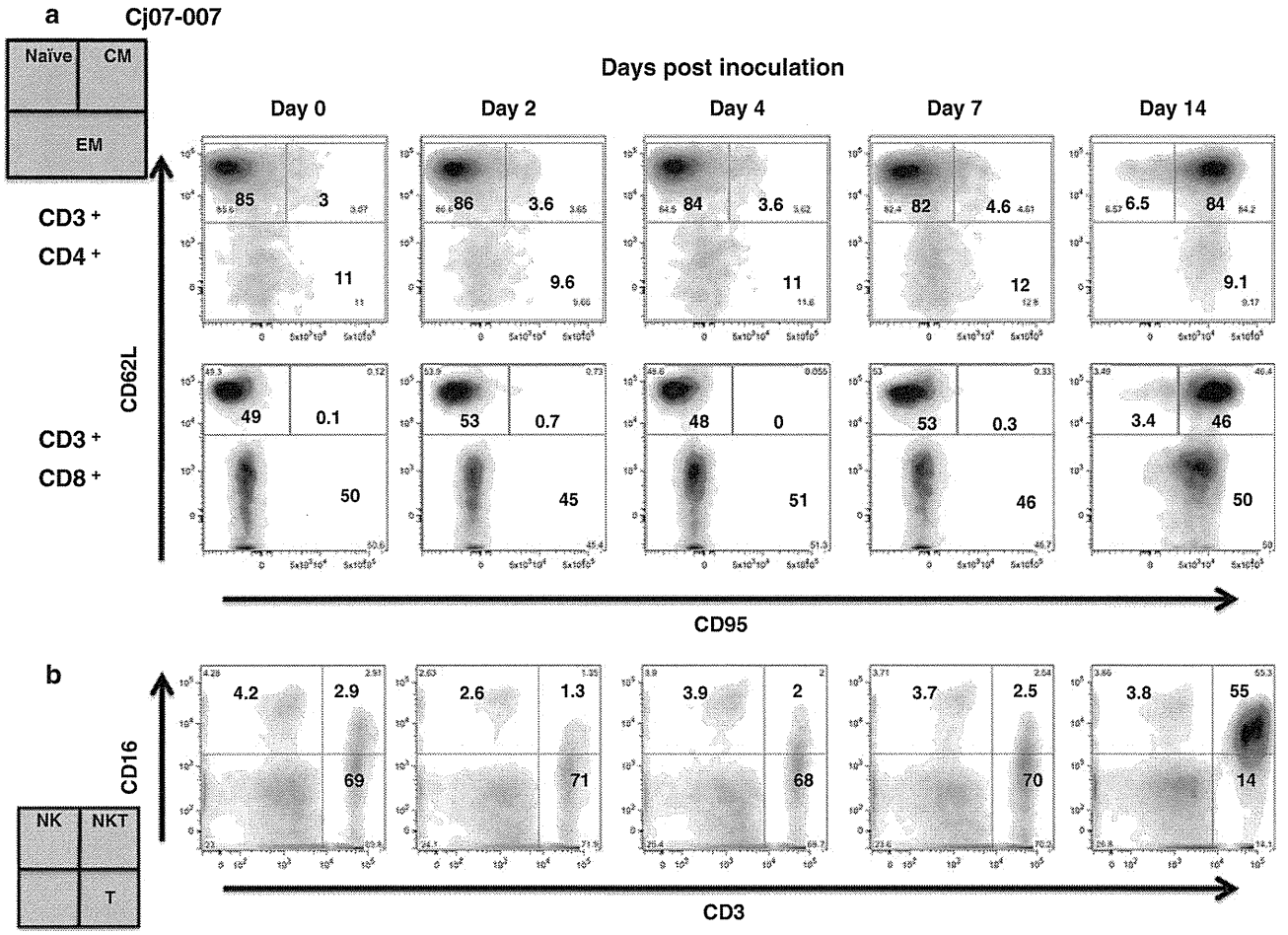

Fig. 6 Profiling of CD4 and CD8 T, NK and NKT cells in marmosets after re-challenge with the DENV-2 DHF0663 strain. Two marmosets that were initially inoculated with 1.8×10^5 PFU of the DHF0663 strain were re-inoculated 33 weeks after the primary challenge with 1.8×10^5 PFU of the same strain. (**a**) Profiling of naïve, central memory, and effector memory CD4 and CD8 T cells in total CD4 and CD8 T cells. (**b**) Profiling of NK and NKT cells in total lymphocytes. (**a-b**) Cj07-007

$CD4^+$ T_N cells decreased strongly at the same time. $CD4^+$ T_{EM} cells maintained their initial levels through the observation period. Similarly, $CD8^+$ T_{CM} and NKT cells clearly increased on day 14 post-inoculation. Importantly, these T cell responses were induced one week after the obvious induction of the neutralizing antibody in the marmosets [24]. These results suggest that the neutralizing antibody may play a critical role in the complete inhibition of the secondary DENV infection.

Discussion

In this study, we demonstrated the dynamics of the central/effector memory T cells and NK/NKT subsets against DENV infection in our marmoset model. First, we characterized the central/effector memory T and NK/NKT subsets in marmosets (Fig. 1). Second, we found that CD4/CD8 central memory T cells and NKT cells had significant responses in the primary DENV infection, and the levels appeared to be dependent on the strain of the virus employed for challenge experiments (Figs. 2–5). Finally, we found delayed responses of CD4/CD8 central memory T cells in the monkeys re-challenged with the same DENV DHF strain, despite the complete inhibition of DENV replication (Figs. 6–7).

The present study shed light on the dynamics of cellular and humoral immune responses against DENV *in vivo* in the marmoset model. Our results showed that cellular immune responses were induced earlier than antibody responses in the primary infection. Thus, our results suggest the possibility that cellular immunity may contribute, at least in part, to the control of primary DENV infection. On the other hand, in the presence of neutralizing antibodies in the re-challenged monkeys [24], delayed (on day 14 after the re-challenge) responses of CD4/CD8 central memory T cells were observed despite the complete inhibition of DENV replication. These results indicate that